

**Multiscale Variability of the Flow During the North American Monsoon
Experiment**

Richard H. Johnson¹, Paul E. Ciesielski, Brian D. McNoldy, Peter J. Rogers, and Richard
K. Taft

Department of Atmospheric Science
Colorado State University
Fort Collins, CO 80523

December 2005

(revised April 2006)

(submitted to *J. Climate*)

¹*Corresponding author address:* Richard H. Johnson, Department of Atmospheric Science, Colorado State University, Fort Collins, CO 80523. E-mail: johnson@atmos.colostate.edu

Abstract

The 2004 North American Monsoon Experiment (NAME) provided an unprecedented observing network for studying the structure and evolution of the North American Monsoon. This paper focuses on multiscale characteristics of the flow during NAME from the large scale to the mesoscale using atmospheric sounding data from the enhanced observing network.

The onset of the 2004 summer monsoon over the NAME region accompanied the typical northward shift of the upper-level anticyclone or monsoon high over northern Mexico into the southwestern U.S., but in 2004 this shift occurred slightly later than normal and the monsoon high did not extend as far north as usual. Consequently, precipitation over the southwestern U.S. was slightly below normal, although increased troughiness over the Great Plains contributed to increased rainfall over eastern New Mexico and western Texas. The first major pulse of moisture into the Southwest occurred around 13 July in association with a strong Gulf surge. This surge was linked to the westward passages of Tropical Storm *Blas* to the south and an upper-level inverted trough over northern Texas. The development of *Blas* appeared to be favored as an easterly wave moved into eastern Pacific during the active phase of a Madden-Julian Oscillation.

On the regional scale, sounding data reveal a prominent sea breeze along the east shore of the Gulf of California, with a deep return flow as a consequence of the elevated Sierra Madre Occidental (SMO) immediately to the east. Subsidence produced a dry layer over the Gulf, whereas a deep moist layer existed over the west slopes of the SMO. A prominent nocturnal low-level jet was present on most days over the northern Gulf. The diurnal cycle of heating and moistening (Q_1 and Q_2) over the SMO was characterized by deep convective profiles in the mid-to-upper troposphere at 1800 LT, followed by stratiform-like profiles at midnight, consistent with the observed diurnal evolution of precipitation over this coastal mountainous region. The analyses in the core NAME domain are based on a gridded dataset derived from atmospheric soundings only, and therefore should prove useful in validating reanalyses and regional models.

1. Introduction

From June through September 2004 the North American Monsoon Experiment (NAME) was conducted over northwestern Mexico and the southwestern United States to investigate the mean structure and variability of the North American summer monsoon. A key element of the NAME observing system was a network of operational and supplemental soundings stretching from central Mexico to the southern United States (Fig. 1). This sounding network, in combination with an array of other observing systems (ships, aircraft, wind profilers, radars, and surface stations), was designed to study the complex and multifaceted properties of the North American summer monsoon: its onset, precipitation characteristics, the Gulf of California (GoC) low-level jet, Gulf surges, easterly waves, tropical cyclone influences, orographic effects, mesoscale convective systems, and the diurnal cycle of convection (Higgins et al. 2005).

While the North American summer monsoon is not as dramatic as its Asian counterpart, it still features several prominent monsoon-like characteristics, e.g., (1) a reversal in the mean low-level flow over the Gulf of California (Badan-Dangon 1991), and (2) areas such as northwestern Mexico receiving a major fraction of their total annual precipitation during the summer season (Douglas et al. 1993; Higgins et al. 1997; Bordoni et al. 2004). The development of the summer monsoon is related to heating and cooling over the elevated terrain of Mexico and the western United States (Krishnamurti 1971; Tang and Reiter 1984). Over Asia the onset of the summer monsoon is concurrent with the reversal of the upper-tropospheric temperature gradient south of the Tibetan Plateau (Flohn 1957; Yanai et al. 1992). Li and Yanai (1996) show that there is a corresponding reversal in this gradient over North America, but it is much weaker. Nevertheless, important regional monsoon features exist over northwestern Mexico and the southwestern United States (see reviews by Douglas et al. 1993; Adams and Comrie 1997; Higgins et al. 2003) and these features are critical for precipitation forecasting and water resource management in this part of North America.

The purpose of this paper is to document the summer 2004 mean flow characteristics and multiscale variability over the NAME domain using data from the NAME sounding network. Particular attention will be given to the kinematic and thermodynamic properties, as well as the apparent heat and moisture sources and sinks, over the interior of the NAME domain using objectively analyzed NAME data. The objective analysis technique does not incorporate model data², so that results (such as vertical motion and heating rates) over the interior of the domain are independent of model influences. The paper will focus on regional changes in the flow accompanying the onset of the summer monsoon; characteristics of Gulf of California wind surges (hereafter Gulf surges); factors influencing Gulf surges, such as easterly waves, upper-level inverted troughs, deep convection, and the Madden-Julian Oscillation (MJO); properties of the sea and land breezes, and the diurnal cycle of convection over the Sierra Madre Occidental (SMO) and surrounding region.

2. Data and analysis procedures

a. Sounding data

The extended NAME sounding network is shown in Fig. 1. It consists of three nested domains: Tier II Array (T2A), covering most of Mexico and the southwestern United States; Tier I Array (T1A), covering the core NAME region where precipitation is modulated by the North American monsoon; and Enhanced Budget Array (EBA), where a denser network of soundings was established to capture heat and moisture budgets in proximity to the rain gauge and radar networks. T2A consists of operational sounding sites of the United States Weather Service and the Mexico Weather Service (Servicio Meteorológico Nacional or SMN), some of which increased their launch frequency during the ten Intensive Observing Periods (IOPs) of NAME, and five additional sounding sites established along the GoC (Puerto Peñasco, Bahia Kino, Los Mochis, Loreto, and the R/V *Altair*). In the EBA, up to six soundings per day were obtained during IOPs in order to study the diurnal cycle of the

²An exception is for several analyses over the large-scale NAME region where reanalysis data are incorporated over the open ocean near the boundary areas of the domain.

flow and convection in the vicinity of the SMO both when significant weather events were occurring and during undisturbed conditions. The launch frequencies for these sites during the interval encompassing nine Intensive Observing Periods (IOPs), 1 July to 15 August, are indicated in Fig. 1.

The National Center for Atmospheric Research S-Band polarimetric (S-Pol) research radar operated within the budget polygon during the period of NAME IOPs. In addition, NCAR Integrated Sounding Systems (ISSs), consisting of Vaisala GPS sounding systems, 915-MHz wind profilers, radio acoustic sounding systems (RASSs), and surface meteorological stations, were operated at Puerto Peñasco, Bahia Kino, and Los Mochis. The ISSs provided high time resolution (30-min) wind profiles reliably in the lowest 2-3 km of the atmosphere. The RASS provided vertical profiles of virtual potential temperature in the lowest 1.25 km. However, the RASS could not operate during the night at Puerto Peñasco and Bahia Kino due to the impact of its high-pitched transmitted signal on the local populace. In addition to these fixed sounding measurements, the NOAA P-3 aircraft conducted ten missions along the Gulf of California to study the low-level jet, Gulf surges, and diurnally varying mesoscale flows.

Sounding quality control procedures patterned after those used in TOGA COARE (Loehrer et al. 1996) have been applied to the raw NAME sounding data. This procedure includes automated internal consistency checks (e.g., gross limit and vertical consistency checks) and the assignment of quality flags. In addition, each of the 7309 soundings from 67 sites was visually inspected up to 100 hPa using skew- T plots for the thermodynamic variables and vertical profiles for the u and v -wind components. Further details and access to quality-controlled datasets are now available at <http://tornado.atmos.colostate.edu/name/>.

b. Other data sources

Surface winds over the GoC and the eastern Pacific are obtained from National Aeronautics and Space Administration's Quick Scatterometer (QuikSCAT), which provides wind estimates nominally twice per day at 25-km horizontal resolution (Liu 2002). SST data

were obtained from the Physical Oceanography Distributed Active Archive Center at the NASA Jet Propulsion Laboratory. Precipitation estimates at 3-h intervals, 0.25° resolution are based on the Tropical Rainfall Measuring Mission (TRMM) 3B42v6 algorithm (Huffman et al. 2005). National Center for Environmental Prediction (NCEP) Reanalysis data at $2.5 \times 2.5^\circ$ resolution (Kalnay et al. 1996) are obtained from NCAR.

c. Objective analysis

In this study gridded fields of horizontal wind components u and v , temperature T , specific humidity q , and geopotential height z at 1° horizontal and 25 hPa vertical resolution have been computed from the quality-controlled sounding data using the multiquadric interpolation scheme of Nuss and Titley (1994). Additional details of the procedure can be found in Ciesielski et al. (2003). These gridded analyses were produced at 00 and 12 UTC over the T2A domain covering $90\text{--}120^\circ\text{W}$, $15\text{--}40^\circ\text{N}$ for the period 1 July to 15 August. For the period with intensive observations from 7 July to 15 August, gridded analyses were computed at 00, 06, 12 and 18 UTC over the T1A domain shown in Fig. 1. To aid the T1A analysis at 06 and 18 UTC on non-IOP days, time-interpolated sondes and profiler data from the ISS sites were used. On IOP days, gridded analyses were produced at 00, 04, 08, 12, 16 and 20 UTC over a domain slightly larger than the EBA from $103\text{--}112^\circ\text{W}$, $23\text{--}29^\circ\text{N}$. Owing to the oceanic data-void regions in T2A, grid points over the Eastern Pacific and Gulf of Mexico were assigned NCEP Reanalysis data (Kalnay et al., 1996). *However, we emphasize that this procedure to enhance the data field was only applied to large-scale T2A analyses so that meaningful results could be obtained over the open ocean where no soundings existed. It was not applied in the interior NAME domains (T1A and EBA), so the results there are completely independent of model data.* In addition, analysis at the surface included observations from METAR stations and QuikSCAT winds over the oceans when available.

The vertical p -velocity ω used in computing the atmospheric budgets was obtained through the kinematic method where horizontal divergence is integrated upward starting at the surface. For the computations in this paper, the condition $\omega = 0$ is assumed. It is

recognized that this assumption is not valid over mountainous terrain; however, since we are still awaiting additional observations (e.g., pibal and aircraft data) to incorporate into our analysis to better define the flow along the slopes of the SMO, we are proceeding with it in this preliminary study. The magnitude of the upward (downward) motion over the SMO will be underestimated by this procedure when there are upslope (downslope) flows. Next, the divergence field is mass balanced in the vertical by assuming adiabatic flow at the tropopause and using a constant divergence correction as suggested by O'Brien (1970). Details on the computation of the apparent heat source Q_1 and apparent moisture sink Q_2 can be found in Johnson and Ciesielski (2000).

Whenever possible, results presented in this paper were created from the gridded analyses described above. For results that extend outside the 1 July - 15 August time frame and the T2A domain, NCEP reanalysis fields were used.

3. Large-scale flow and its variability

a. Upper-level flow and precipitation

The onset phase of the North American Monsoon (NAM) is characterized by a northward advance of precipitation along the western slopes of the SMO during June with precipitation arriving in southern Arizona by the end of the first week in July (Douglas et al. 1993; Adams and Comrie 1997; Higgins et al. 1999). This advance is accompanied by the northward migration of an upper-level anticyclone, which leads to a shift from westerly to easterly upper-tropospheric flow over the region. Bryson and Lowry (1955) first noted this shift and showed that it was accompanied by a widespread outbreak of rains over Arizona. It has also been simulated in regional modeling studies (e.g., Saleeby and Cotton 2004; Xu et al. 2004). This wind shift can be seen to be more-or-less permanent around 10 July in Fig. 2, a time-longitude plot of the NCEP Reanalysis 300-hPa zonal wind at the latitudes of northern Mexico (25-30°N) centered over the NAME domain. Correspondingly, the onset of the summer monsoon in southern Arizona occurred near this date. This onset can be seen

in a time series of precipitation (center panel, Fig. 2) over an area in northern Sonora and southern Arizona (see box in Fig. 4a). As indicated in Fig. 2, the wind shift in 2004 occurred about ten days later than the 25-year NCEP Reanalysis mean, consistent with observations by forecasters during the NAME 2004 field phase of a slightly delayed onset. This finding is also consistent with Castro et al. (2001), who showed that during El Niño years (2004 was a weak El Niño year; Levinson et al. 2005), monsoon onset is late. However, as reported by Higgins and Shi (2000), it falls within the range of mean onset dates ($7 \text{ July} \pm 10.1 \text{ days}$) they determined for Arizona/New Mexico for the period 1948-1996. An intrusion of westerlies that occurred in mid-to-late August was initially associated with an increase in precipitation, but then was followed by drastically reduced rainfall.

Also shown in Fig. 2 is the time series of 300-hPa meridional wind. A notable feature of this plot, when comparing it with the zonal wind plot, is the transition from eastward-propagating disturbances during pre-onset westerly phase to westward-propagating disturbances during the post-onset easterly phase. Westward propagation can once again be seen in the mid-to-late August westerly phase. During the westerly phase, these disturbances are associated with eastward-moving midlatitude baroclinic or Rossby waves. However, during the easterly phase they are related to upper-level inverted troughs whose likely origins are ‘Rossby-wave breaking’ or thinning midlatitude troughs that advect equatorward and anticyclonically around the monsoon high (Thorncroft et al. 1993). The latter disturbances are sometimes referred to as tropical upper-tropospheric troughs or TUTTs (Sadler 1967). The axes or centers of TUTTs have been shown by Whitfield and Lyons (1992) to frequently track from the Caribbean and Gulf of Mexico across Mexico, and then typically weaken when they reach the eastern Pacific. A prominent upper-level trough can be seen passing through the EBA around 13 July and yet another around 23 July. Both were associated with strong Gulf surges, although their exact role in these surges is yet to be determined.

The 1 July–15 August 300-hPa mean flow, 2004 height anomalies from the 25-year mean (1980-2004), and potential vorticity (PV) variance over the T2A domain are shown in Fig.

3. As indicated by the height anomalies, the 300-hPa anticyclone was shifted south of its normal position in 2004 and correspondingly, precipitation over the southwestern U.S. was below normal (Fig. 4b). This pattern is consistent with Castro et al. (2001), who found that El Niño years favor a southward-displaced monsoon ridge and below-average early-summer rainfall over the Southwest. This anomalous pattern was even more prominent during the June pre-onset period, with a strong negative height anomaly centered over northern Mexico extending over the entire country (not shown).

A map of the mean precipitation during NAME (Fig. 4a) shows maximum rainfall in Mexico along the western slopes of the SMO. This satellite-based rainfall map compares favorably to estimates from the NAME Enhanced Rain Gauge Network (NERN, D. Gochis, personal communication, 2004) and the Climate Prediction Center (CPC) U.S.-Mexico merged precipitation dataset (Higgins et al. 2000)(not shown). Precipitation during 2004 was above normal throughout much of this region, particularly in the area of the EBA (Fig. 4b). Maxima in PV variance occurred upstream and downstream of the ridge axis; the one over Texas being associated with the frequent occurrence of TUTT-like, upper-level troughs there and the one over southern California associated with midlatitude westerly troughs encroaching on the monsoon region from the west, perhaps associated with the frequent occurrence of cutoff lows in this region (Nieto et al. 2005). The prevalence of negative 300-hPa height anomalies to the lee of the Rocky Mountains is consistent with the observations during NAME of a strong trough over the central U.S. (Levinson et al. 2005) and of frequent ‘back-door’ cold fronts that led to positive precipitation anomalies over eastern New Mexico and western Texas (Fig. 4b).

b. Lower-tropospheric flow

Studies by Erickson (1971), Kelley and Mock (1982), and Whitfield and Lyons (1992) show that upper-level inverted troughs or cold lows have a maximum positive vorticity anomaly near 200 hPa, weakening to near zero at 700 hPa, and a maximum cold anomaly near 300 hPa. These disturbances are often distinct from tropical easterly waves, which

typically track across the NAME region farther to the south (Stensrud et al. 1997; Raymond et al. 1998; Molinari et al. 2000; Petersen et al. 2003). However, Fuller and Stensrud (2000) note that some of the easterly waves they tracked may have originated at midlatitudes; hence, they may be linked to TUTT disturbances. A time-longitude diagram of the 700-hPa meridional wind averaged over 15-25°N (Fig. 5, from the NCEP Reanalysis) shows a sequence of easterly waves traversing the Caribbean and reaching the eastern Pacific, culminating in several instances as tropical cyclones. The first of these that significantly affected weather in the NAME region, Tropical Storm *Blas*, developed from an easterly wave that crossed central America (National Hurricane Center, Tropical Cyclone Report, 2004) and contributed to the first strong Gulf surge on 13 July (to be discussed later).

There is evidence to indicate that the tropical cyclone activity shown in Fig. 5 is modulated on the time scale of the Madden-Julian Oscillation (MJO; Madden and Julian 1971). This association is revealed in Fig. 6, time-longitude plots of the equator-to-10°N averaged 850-hPa and 200-hPa winds over the Pacific Ocean. Outbreaks of tropical cyclone activity in the eastern Pacific (black dots in Fig. 6) occur at times when 850-hPa westerly wind anomalies complete their transit of the Pacific Ocean. This signal of the MJO (or convectively coupled Kelvin waves; Straub and Kiladis 2002) is also apparent as a weakening or disappearance of the 200-hPa westerlies (right panel, Fig. 6) over the eastern Pacific. These results are consistent with Maloney and Hartmann (2000) and Higgins and Shi (2001), who showed that tropical cyclogenesis is favored during the active periods of the MJO when there is greater MJO-induced cyclonic shear vorticity at low levels, reduced vertical shear, and increased divergence aloft. Molinari et al. (2000) showed that easterly waves arriving in the eastern Pacific from the Atlantic and Caribbean are more likely to develop into tropical cyclones when the active phase of the MJO is present in that region.

Studies by Hales (1974), Brenner (1974), Carleton (1986), Douglas et al. (1993), Schmitz and Mullen (1996), Berbery (2001) have shown that the primary moisture source for monsoon convection over the SMO and southwestern Arizona is from flow along the GoC and the

eastern Pacific, although the contribution from the latter source has been uncertain due to the lack of observations over Baja California. Observations from NAME have provided an improved description of the flow along the GoC, although as of this writing additional pibal and aircraft data that will enable an even better definition of this flow have not yet been processed. Therefore, rather than present maps of the low-level flow, which at this stage closely resemble those of Douglas (1995), we show the 1 July–15 August mean QuikSCAT surface winds and SST (Fig. 7). The dominant features include northerly flow over cool water around the eastern Pacific subtropical anticyclone and a bifurcation of the flow at the mouth of the GoC, with one branch extending up the Gulf over very warm water and another turning to the southeast. The mean flow is strongly divergent at the mouth of the GoC, which along with cool-air advection implied by the SST gradient there, accounts for minimal seasonal-mean precipitation in this location (Fig. 4a).

The twice-per-day resolution of the QuikSCAT data permits detection of day-to-day variability in the GoC flow and, in particular, Gulf surges. The component of the QuikSCAT surface wind along the axis of the GoC and a 2-3° coastal strip to its south from June through September is shown in Fig. 8. Also shown in this figure is a time series of the surface pressure difference between Mazatlan near the mouth of the GoC and Yuma to the north. Episodic increases in wind speed along the Gulf at 5-10 day intervals can be seen, in most cases originating at the southern tip of Baja and subsequently propagating northward. The majority of these wind increases (Gulf surges) are accompanied by increases in the north-to-south pressure gradient along the GoC (Brenner 1974). The pressure-gradient increases typically arise from pressure rises in the south preceding those in the north within the desert heat low. This sequence of events can be seen in Fig. 9, a time series of the surface pressure anomalies at the three ISS sites. Referring to the Gulf surge of 13 July, one of the strongest in NAME, it is seen from Fig. 9 that pressure rises first occur at Los Mochis in the south, then Bahia Kino, and finally at Puerto Peñasco. This surge event was briefly discussed in Higgins et al. (2006) and will be treated in more detail in a future paper. However, a striking

feature from Fig. 9 is that, ignoring the slight phase shifts, the pressures along the GoC vary more-or-less in unison when viewed on longer (weekly) time scales. This result suggests that it is usually the same synoptic regime that controls the pressure field along the entire GoC.

Seen in Fig. 8 are several instances where southerly meridional flow extends to the south of the GoC; these cases are typically linked to the passage of tropical cyclones to the south and are labeled by the names of associated tropical cyclones. In a study of nine years of Gulf surges at Empalme, Douglas and Leal (2003) found many surges to be associated with tropical cyclone passage to the south of the GoC. Also in Fig. 8, there are several surges confined to the northern half of the GoC, as have been found previously (Hales 1972; Stenrud et al. 1997). The origin of these northern GoC surges has been generally attributed by these authors and others to downdraft outflows from mesoscale convective systems in this region.

The Gulf surge on 13 July associated with TS *Blas* was accompanied by the first major transport of moisture north of 30°N into the western U.S. (Fig. 10). Values of total-column precipitable water exceeding 24 mm can be seen to extend all the way to 40°N following this surge event.

4. Flow along the Gulf of California

a. Regional kinematic and thermodynamic properties

Profiles of the 7 July–15 August mean zonal and meridional wind, potential temperature, and relative humidity (throughout the paper with respect to ice at temperatures below freezing), along with standard deviations of the daily-averaged values, over both the land and gulf portions of the EBA are shown in Fig. 11. The EBA is divided into these regions because of the sharply contrasting convective behavior between the two, namely, a persistent diurnal cycle of strong convection over land and weak, infrequent convection over the gulf. The mean zonal flow is easterly (except at low levels over the gulf) since this region near the southern GoC is south of the upper-level ridge axis, and the meridional flow is mostly southerly, more so over the gulf nearer the western periphery of the ridge. Standard deviations are greatest

near the outflow level (150-200 hPa) due to the stronger winds there, variability in convective activity over the SMO, and the occurrence of upper-level troughs. There is a local maximum in relative humidity near 600 hPa and another near the surface over both land and ocean, with a third peak near 800 hPa over the ocean (to be discussed in more detail later). The standard deviation in relative humidity is greater in the upper troposphere over the gulf due to the infrequent passage of convective systems there, as opposed to the daily occurrence of convection over land. The θ standard deviation is slightly greater in the lowest 2-3 km as a result of the impacts of Gulf surges and variable convective activity on the low-level temperature field. While the differences in the basic fields in Fig. 11 between land and gulf are relatively small, we will see later that fields involving their gradients (e.g., divergence, vertical motion, heating, and moistening shown later in Fig. 19) are not small.

A vertical cross section of the 1 July–15 August mean flow along the axis of the GoC (AG line shown in Fig. 4a) is shown in Fig. 12. Displayed are isentropes, mean flow along the plane of the section, and relative humidity. At low levels there is a shallow moist layer near the surface topped by a local maximum in the southeasterly flow and a deep layer of subsidence. This feature is the nocturnal low-level jet (LLJ) as it appears in the daily-mean profile. It is strongest in the northern GoC and weakens toward the south, consistent with the findings by Douglas (1995) and the QuikSCAT surface winds shown in Fig. 7. ISS data from Puerto Peñasco show the diurnal variation of this LLJ (Fig. 13), which was observed on 66% of the days at this site. A wind maximum of about 8 m s^{-1} occurs at $\sim 950 \text{ hPa}$ ($\sim 400\text{-}500 \text{ m}$) at about 0600 LT, in general agreement with the Douglas (1995) study of the LLJ at Yuma. The primary variation in the low-level relative humidity along the Gulf (Fig. 12) is a gradual drying in the lowest kilometer from south to north, as also found by Douglas et al. (1993) and Stensrud et al. (1995). In addition, there is a lower-tropospheric gradient in potential temperature, with cooler air to the south, as expected with the desert heat low to the north and a marine environment in the southern Gulf. Considering that the mean low-level monsoon flow is from the southeast approximately along the axis of the gulf

(Douglas et al. 1993), the downward-sloping isentropes (implying subsidence) are consistent with increased drying in the north.

Another layer of strong southeasterly, along-Gulf flow can be seen near 600 hPa coincident with a layer of higher relative humidity (Fig. 12). This feature is the westward extension of the Bermuda high. As shown by Douglas et al. (1993), the moisture source for this layer is from vertical transport due to afternoon deep convection along the west slope of the SMO and subsequent westward advection. Finally, there is another layer near the tropopause of enhanced southeasterly flow associated with the monsoon high aloft (Fig. 3).

The source of the moist layer near 600 hPa in Fig. 12 can be seen in Fig. 14, a vertical cross section perpendicular to the SMO over the southern GoC (see Fig. 4a for position). In this figure, strong flow toward the west can be seen centered near 600 hPa again coincident with a moist layer, clearly showing the westward advection of moisture associated with deep convection over the SMO, as Douglas et al. (1993) proposed. Abundant moisture also exists along the west slope of the SMO, but is missing from the area of the mountain crest. It is possible that the lack of high relative humidity near the crest of the SMO in the analysis is an artifact and a consequence of the absence of observations in this part of the domain (Fig. 1). Conceivably, the high relative humidities on the west slope could extend upward and meet with high values in the midtroposphere given the presence of deep convection, but data are lacking to show this feature. The lighter precipitation on the east slope of the SMO relative to the west is, in part, a consequence of the drier conditions there (Fig. 14), but also may be related to the mean easterly flow that advects storms westward. At low levels, there is a mean onshore flow in the southern GoC, as also seen in Douglas et al. (1993).

Also shown in Fig. 14 is the divergence field, whose main features are convergence above the mountain crest and divergence aloft between 150 and 200 hPa³ There is also a shallow

³One would expect high values of relative humidity (with respect to ice) in the divergent outflow layer aloft; however, they are not seen in this figure, nor in other figures. Continuing analysis of NAME sounding data quality has revealed a significant dry bias in the SMN soundings peaking at 30-40% in the 100-150 hPa layer. Work is underway to determine the nature of this bias and develop a humidity correction algorithm, but that work has not been completed in time for this paper.

layer of strong divergence over the GoC, reflecting the dominance of the sea breezes over the GoC at this time of year associated with both the SMO and the mountain range along Baja California. The layer of convergence just above (near 800 hPa) is partly associated with converging airflows in the sea breeze return flow. The resulting subsidence over the Gulf, perhaps aided by orographically induced sinking of the easterly flow to the lee of the SMO, serves to maintain the relatively dry lower troposphere there (Fig. 12) despite the very warm waters (Fig. 7). The return flow of a sea breeze over flat terrain normally begins at 1-2 km above ground level (e.g., Anthes 1978; Banta et al. 1993). The high terrain of the SMO extends this return flow upward to higher levels, as also found in the numerical simulations of Stensrud et al. (1995; see their Fig. 14), although the precise level of the return flow is uncertain due to the absence of inland soundings.

Further evidence of this “deep sea breeze” circulation can be seen in Fig. 15, the diurnal variation of the flow (anomalies of the wind and relative humidity from the 24-h means) normal to the coastline at Los Mochis, which of the ISS sites is situated closest to the mountains. An afternoon sea breeze peaks near 1800 LT, while there are offshore flow maxima near 600 and 150 hPa over a broad period in the afternoon and evening. Just how the return flow from the sea breeze is distributed vertically is not completely clear from these analyses; however, perhaps a part of it is actually from the thunderstorm outflows aloft. The boundary layer dries out in the afternoon due to surface heating, but moistening occurs during the evening and at night from surface evaporation and offshore flow bringing moisture westward from the SMO. The 150-hPa easterly wind anomaly in the evening is associated with outflow aloft from afternoon/evening convection over the SMO, which brings high-level moisture over Los Mochis during the nighttime hours. There is also a diurnal modulation of the flow near 800 hPa (onshore in the evening, offshore in the morning). This feature may be associated with surges of offshore flow behind convective systems that typically pass through Los Mochis during the nighttime hours. Similar features to those observed in Fig. 15 can be seen at Bahia Kino, but the circulations in the mid- and upper-troposphere are

weaker because the station is farther from the mountains and the mean precipitation over the SMO at that latitude is less (Fig. 4a).

Time series of u , v , relative humidity, and temperature deviation from the mean for the gulf portion of the EBA (Fig. 1) are shown in Fig. 16 for the 7 July–15 August period, which includes nine IOPs. The shift in the 300-hPa westerlies to easterlies around 10 July noted earlier in Fig. 2 can be seen in this figure, although at higher levels there is a return to westerlies for several days due to outflow aloft from TS *Blas* which passed to the west of Baja. The entire upper troposphere was dominated by easterlies after 18 July, with brief interruptions by westerlies at the end of July and in mid-August. The meridional wind fluctuated between northerly and southerly aloft in association with the passage of upper-level troughs (Fig. 2) and the movement of upper-level anticyclones. At low levels, the flow was generally southerly, with marked enhancements of the southerly flow on 12-13 and 23-24 July, and on several other occasions. The increased southerlies during these two periods were accompanied by moistening of the entire troposphere as well as lower-tropospheric cooling (lower panels, Fig. 16). These events were two of the strongest Gulf surges during NAME (Fig. 8), the first of which was discussed in Higgins et al. (2006). Note that the strong low-level cooling was preceded by strong warming and drying, as also found by Douglas and Leal (2003) in their study of surges at Empalme. The same time series in Fig. 16 have been constructed for the land-portion of the EBA (not shown), but the results are similar to that over the water except that the signatures of the Gulf surges are not as well defined as would be expected over land. These surges will be discussed in greater detail in a forthcoming paper.

b. Derived fields over the Enhanced Budget Array

To demonstrate the veracity of the gridded-analysis fields, the 500-hPa vertical motion is plotted in Fig. 17 along with the TRMM 3B42v6 mean precipitation for the period 1 July–15 August. Since the majority of the precipitation in this region is associated with deep convection, the good agreement between these two fields (over T1A where the data

coverage is best) indicates that the sounding network is doing a reasonable job of capturing the structure of the divergence and vertical motion fields over this region.

Time series of divergence, vertical motion, the apparent heat source, and the apparent moisture sink (Yanai et al. 1973) are shown in Fig. 18, this time for the land-portion of the EBA since convection is greatest there (data below 850 hPa, the average terrain elevation, are omitted). From the standpoint of budget studies of convection, it is perhaps fortunate that a positive precipitation anomaly was situated over the EBA (Fig. 4b). From these results, it can be seen that there were maxima of upper-level divergence, low-level convergence, and upward vertical motion during the majority of IOPs, which is gratifying since most IOPs were designed to capture disturbed weather and deep convection. The mean divergence maximum aloft was near 175 hPa (Fig. 19), although from Fig. 18 this level can be seen to vary from 125 to 200 hPa. Multiple layers of convergence occurred throughout the low-to-midtroposphere, although the greatest values in the mean (Fig. 19) are below the crest of the SMO ($\sim 3\text{-}4$ km). Upward motion typically peaked near 350 hPa, similar to the findings for the western Pacific (e.g., Yanai et al. 1973; Lin and Johnson 1996 for the Tropical Ocean Global Atmosphere Coupled Ocean-Atmosphere Response Experiment or TOGA COARE) and the central U.S. (Gallus and Johnson 1991), but higher than the eastern Atlantic (Thompson et al. 1979 for the GARP Atlantic Tropical Experiment or GATE). Correspondingly, there was a peak in the mean Q_1 in the mid-to-upper troposphere (Fig. 19). However, a mean cooling was present in the lower troposphere below 750 hPa. This cooling, not seen in budget studies over moist, tropical oceanic regions (e.g., Yanai et al. 1973; Thompson et al. 1979), is characteristic of Q_1 profiles over continental regions (e.g., Gallus and Johnson 1991) where relatively dry conditions (compared to the Tropics) in the lower troposphere contribute to enhanced precipitation evaporation. This effect can also be seen in the Q_2 profiles (Figs. 18 and 19) where moistening is observed in the lower troposphere. While these results are consistent with past studies over land, they must be regarded as tentative and awaiting further analysis using additional sounding data. Determination of the vertical profile of heating in the NAME

monsoon region is important since there is considerable uncertainty in this profile based on models and large-scale circulation is sensitive to the vertical heating distribution (Barlow et al. 1998).

Also shown in Fig. 19 are the mean profiles over the Gulf portion of the EBA. There is a striking difference in all of the profiles from those over land with only weak upward motion present, consistent with the small amount of precipitation observed in this region (Fig. 4a). The Q_2 profile over the water is suggestive of stratiform precipitation (drying aloft, moistening at low levels); however, more work is underway to relate these profiles to S-Pol radar observations of precipitation in the EBA.

As a first attempt to understand the role of the diurnal cycle in producing the mean profiles in Fig. 19, each of the fields in the land portion of the EBA are shown at four times per day in Fig. 20. As expected in this domain centered over the SMO, a strong diurnal cycle is evident with an upward motion and Q_1 peaking at 1800 LT. By midnight, Q_1 , and Q_2 profiles are more characteristic of stratiform precipitation with heating and drying in the upper troposphere, and cooling and moistening in the lower troposphere below the 0°C level (Houze 1982; Johnson and Young 1983). In the early morning (0600 L), there is mostly cooling in the lower troposphere, but by noon, there is heating and drying at low levels in response to sensible heating of the SMO, developing clouds, and shortwave absorption by the atmosphere.

5. Summary and Conclusions

Sounding data obtained during the 2004 North American Monsoon Experiment (NAME) have permitted a documentation of the structure and properties of the flow within the North American Monsoon in a detail heretofore not possible. Observations from rawinsondes and wind profilers have been quality controlled, merged, and processed into gridded datasets covering nested tiers across the entire NAME region. This paper reports on preliminary results from these gridded datasets, which have only recently become available. Analyses over the interior NAME region (the Tier 1 Array and Enhanced Budget Array or EBA) are

completely independent of model data, so the gridded fields should be of value for validating reanalyses and other modeling studies. Evidence of the reliability of the gridded analyses is contained in a comparison of the 500-hPa vertical motion field with independent TRMM precipitation estimates for the 46-day experiment mean, which shows very good agreement over the NAME domain.

Some of the findings of this study are confirmatory of past work, while some are new. Several of the new findings are as follows.

- Gulf of California (GoC) surges have been documented in unprecedented detail with the NAME dataset. Although only a portion of the findings are reported here (additional results utilizing wind profiler observations are found in Higgins et al. 2006), the full complement of NAME observations reveals the multiscale characteristics of these phenomena. In a large-scale context, their timing is linked to the arrival in the eastern Pacific of the active phase of the Madden-Julian Oscillation (MJO). On a regional scale, QuikSCAT observations show strong southerly surface wind accelerations associated with these surges in response to increasing pressure gradients along the GoC. Some surges are confined to the GoC itself, but those extending farther south are in most cases associated with the passage of tropical cyclones well to the south of the GoC. The NAME sounding network captured the kinematic and thermodynamic properties of two strong surges (on 13 and 23 July), both preceded by strong low-level warming and drying, and followed by strong cooling and moistening. A detailed investigation of the 13 July surge using wind profiler, upper-air, and surface data has recently been completed (Rogers and Johnson 2006).
- The enhanced sounding network in the core of the NAME domain has enabled a documentation of the regional flow characteristics over the Sierra Madre Occidental (SMO) and nearby GoC. At the latitudes of the southern GoC, the mean flow normal to the GoC below 400 hPa is toward the west over the high terrain of the SMO with a broad jet centered near 600 hPa and a positive anomaly in relative humidity associated with

convection over the SMO. Below 900 hPa to the west of the SMO, there is a mean on-shore flow toward higher terrain. A layer of lower-tropospheric convergence is centered over the western slope of the Sierra Madre Occidental (SMO) colocated with a layer of strong divergence aloft between 150 and 200 hPa reflecting the presence of intense afternoon and evening convection over the SMO. These flows vary significantly over the diurnal cycle.

- Computations of divergence, vertical motion, Q_1 , and Q_2 over the land and gulf portions of the EBA show starkly contrasting time-mean profiles. Over the land (which includes the SMO), there is low-level convergence, upper-level divergence, deep upward motion, and strong heating in the upper troposphere. Over the gulf, convection appears to be rare with only weak upward motion principally in the lower troposphere.
- The diurnal cycle of convection over the SMO, determined from computations of the apparent heat source Q_1 and apparent moisture sink Q_2 , is characterized by deep convective heating in the mid-to-upper troposphere at 1800 LT, followed by stratiform-like heating and moistening profiles at midnight. Unlike observations from experiments such as GATE and TOGA COARE, cooling is observed in the lower troposphere in the mean profiles of the apparent heat source Q_1 , likely due to more evaporative cooling from drier conditions at low levels over land compared to the those over tropical oceans.

Findings of this study specific to the 2004 monsoon season and confirmatory of past results are the following.

- In agreement with past studies, the onset of the 2004 summer monsoon over the NAME region accompanied a northward shift of the upper-level anticyclone or monsoon high over northern Mexico into the southwestern U.S., but this shift occurred about ten days later than the long-term mean. The late onset is consistent with previous findings of late monsoon onsets during El Niño (2004 was a weak El Niño year).

- In 2004 the mean position of the monsoon high was south of normal, with below-normal precipitation over northern Sonora and Arizona, and enhanced precipitation to the south. Enhanced troughiness was observed over the central Plains of the U.S., and correspondingly, above-normal precipitation occurred in eastern New Mexico and western Texas due to frequent ‘back-door’ cold fronts.
- The timing of the monsoon onset in 2004 in northern Sonora and Arizona was influenced by disturbances on multiple scales: a strengthening of the heat low over the desert Southwest, tropical cyclone *Blas* (which developed from an easterly wave from the Atlantic and Caribbean), an upper-level trough moving across northern Mexico, and the active phase of a Madden-Julian Oscillation arriving in the eastern Pacific.
- The mean flow along the GoC is characterized by a shallow moist layer and a low-level southerly jet, strongest over the northern gulf, surmounted by subsidence and a relatively dry layer between 925 and 750 hPa. Above this there is a moist layer and enhanced southerly flow peaking near 600 hPa reflecting the presence of the western periphery of the Bermuda high. The latter moist layer is likely a reflection of westward transport of moisture from evening convection over the SMO (Douglas et al. 1993).
- A nocturnal low-level jet is observed on 66% of the days over the northern GoC (at Puerto Peñasco with peak winds at 0600 LT of about 8 m s^{-1} at $\sim 950 \text{ hPa}$ ($\sim 400\text{-}500 \text{ m}$), in general agreement with Douglas (1995).

This study is intended to provide a brief overview of the flow on multiple scales ranging from the large scale down to the mesoscale in association with the 2004 NAME field experiment. Convection, Gulf surges, and other regional-scale and local phenomena are modulated by and interact with flows over this wide range of scales, but it is beyond the scope of this study to explore these relationships in detail. Further work is underway incorporating data from additional sources to investigate these various and complex aspects of the North Amer-

ican Monsoon system. In addition, efforts are proceeding to determine humidity corrections for NAME soundings and to incorporate these corrections into the gridded analyses.

6. Acknowledgments

This research has been supported by the National Science Foundation, Mesoscale Dynamic Meteorology Program, under Grant. No. ATM-0340602 and the National Oceanic and Atmospheric Administration, Office of Global Programs, under Grant No. NA17RJ1228. The comments of three anonymous reviewers are appreciated.

REFERENCES

- Adams, D. K., and A. C. Comrie, 1997: The North American monsoon. *Bull. Amer. Meteor. Soc.*, **78**, 2197–2213.
- Anthes, R. A., 1978: The height of the planetary boundary layer and the production of circulation in a sea breeze model. *J. Atmos. Sci.*, **35**, 1231–1239.
- Badan-Dangon, A., C. E. Dorman, M. A. Merrifield, and C. D. Winant, 1991: The lower atmosphere over the Gulf of California. *J. Geophys. Res.*, **96**, (C9), 877–896.
- Banta, R. M., L. D. Olivier, and D. H. Levinson, 1993: Evolution of the Monterey Bay sea-breeze layer as observed by pulsed Doppler lidar. *J. Atmos. Sci.*, **50**, 3959–3982.
- Barlow, M., S. Nigam, E. H. Berbery, 1998: Evolution of the North American Monsoon System. *J. Climate*, **11**, 2238–2257.
- Berbery, E. H., 2001: Mesoscale moisture analysis of the North American monsoon. *J. Climate*, **14**, 121–137.
- Bordoni, S., P. E. Ciesielski, R. H. Johnson, B. D. McNoldy, and B. Stevens, 2004: The low-level circulations of the North American Monsoon as revealed by QuikSCAT. *Geophys. Res. Lett.*, **31**, L10109,doi:10.1029/2004GL020009.
- Brenner, I. S., 1974: A surge of maritime tropical air- Gulf of California to the southwestern United States. *Mon. Wea. Rev.*, **102**, 375–389.
- Bryson, R. A., and W. P. Lowry, 1955: Synoptic climatology of the Arizona summer precipitation singularity. *Bull. Amer. Meteor. Soc.*, **36**, 329–339.

- Carleton, A. M., 1986: Synoptic-dynamic character of “bursts” and “breaks” in the southwest U.S. summer precipitation singularity. *J. Climatol.*, **6**, 605–623.
- Castro, C. L., T. B. McKee, and R. A. Pielke Sr., 2001: The relationship of the North American monsoon to tropical and north Pacific sea surface temperatures as revealed by observational analyses. *J. Climate*, **14**, 4449–4473.
- Ciesielski, P. E., R. H. Johnson, P. T. Haertel and J. Wang, 2003: Corrected TOGA COARE sounding humidity data: Impact on diagnosed properties of convection and climate over the warm pool. *J. Climate* **16**, 2370–2384.
- Douglas, M. W., 1995: The summertime low-level jet over the Gulf of California. *Mon. Wea. Rev.*, **123**, 2334–2347.
- Douglas, M. W., R. A. Maddox, K. Howard, and S. Reyes, 1993: The Mexican monsoon. *J. Climate*, **6**, 1665–1677.
- Douglas, M. W., and J. C. Leal, 2003: Summertime surges over the Gulf of California: Aspects of their climatology, mean structure, and evolution from radiosonde, NCEP Reanalysis, and rainfall data. *Weather and Forecasting*, **18**, 55–74.
- Erickson, C. O., 1971: Diagnostic study of a tropical disturbance. *Mon. Wea. Rev.*, **99**, 67–78.
- Flohn, H., 1957: Large-scale aspects of the “summer monsoon” in South and East Asia. *J. Meteor. Soc. Japan*, 75th Ann. Vol., 180–186.
- Fuller, R. D., and D. J. Stensrud, 2000: The relationship between tropical easterly waves and surges over the Gulf of California during the North American monsoon. *Mon. Wea. Rev.*, **128**, 2983–2989.

- Gallus, W. A., Jr., and R. H. Johnson, 1991: Heat and moisture budgets of an intense midlatitude squall line. *J. Atmos. Sci.*, **48**, 122–146.
- Hales, J. E., Jr., 1972: Surges of maritime tropical air northward over the Gulf of California. *Mon. Wea. Rev.*, **100**, 298–306.
- Hales, J. E. Jr., 1974: Southwestern United States summer monsoon source–Gulf of Mexico or Pacific Ocean?. *J. Appl. Meteor.*, **13**, 331–342.
- Higgins, R. W., and W. Shi. 2000: Dominant factors responsible for interannual variability of the summer monsoon in the southwestern United States. *J. Climate*, **13**, 759–776.
- Higgins, R. W., and W. Shi, 2001: Intercomparison of the principal modes of interannual and intraseasonal variability of the North American Monsoon System. *J. Climate*, **14**, 403–417.
- Higgins, R. W., Y. Yao, and X. L. Wang. 1997: Influence of the North American monsoon system on the U.S. summer precipitation regime. *J. Climate*, **2600–2622.**,
- Higgins, R. W., Y. Chen, and A. Douglas, 1999: Interannual variability of the North American warm season precipitation regime. *J. Climate*, **12**, 653–680.
- Higgins, R. W., W. Shi, E. Yarosh, and R. Joyce, 2000: Improved US precipitation quality control system and analysis. NCEP/Climate Prediction Center ATLAS No. 7, <http://www.cpc.ncep.noaa.gov>.
Datasets available through www.cdc.noaa.gov.
- Higgins, R. W., and CoAuthors, 2003: Progress in Pan American CLIVAR research: The North American Monsoon System. *Atmósfera*, **16**, 29–65.

- Higgins, R. W., and CoAuthors, 2006: The North American Monsoon Experiment (NAME) 2004 field campaign and modeling strategy. *Bull. Amer. Meteor. Soc.*, **87**, 70–94.
- Houze, R. A., Jr., 1982: Cloud clusters and large-scale vertical motion in the tropics. *J. Meteor. Soc. Japan*. **60**, 396–410.
- Huffman, G. J., R. F. Adler, S. Curtis, D. T. Bolvin, and E. J. Nelkin, 2005: Global rainfall analyses at monthly and 3-hr time scales. Chapter 4, *Measuring Precipitation from Space: EURAINSAT and the Future*, V. Levizzani, P. Bauer, and J. Turk, Eds., Springer Verlag (Kluwer Academic Pub. B.V.), Dordrecht, The Netherlands, (in press)
- Johnson, R. H., and G. S. Young, 1983: Heat and moisture budgets of tropical mesoscale anvil clouds. *J. Atmos. Sci.*, **40**, 2138–2147.
- Johnson, R. H., and P. E. Ciesielski, 2000: Rainfall and radiative heating rate estimates from TOGA-COARE atmospheric budgets. *J. Atmos. Sci.*, **57**, 1497–1514.
- Kalnay, E., and Coauthors, 1996: The NCEP/NCAR 40-Year Reanalysis Project. *Bull. Amer. Meteor. Soc.*, **77**, 437–471.
- Kelley, W. E., and D. R. Mock, 1982: A diagnostic study of upper tropospheric cold lows over the western North Pacific. *Mon. Wea. Rev.*, **110**, 471–480.
- Krishnamurti, T. N., 1971: Tropical east-west circulations during the northern monsoon. *J. Atmos. Sci.*, **28**, 1342–1347.
- Levinson, D. H., and CoAuthors, 2005: State of the climate in 2004. *Bull. Amer. Meteor. Soc.*, **86**, S1–S86.

- Li, C., and M. Yanai, 1996: The onset and interannual variability of the Asian summer monsoon in relation to land-sea thermal contrast. *J. Climate*, **9**, 358–375.
- Lin, X., and R. H. Johnson, 1996: Heating, moistening and rainfall over the western Pacific warm pool during TOGA COARE. *J. Atmos. Sci.*, **53**, 3367–3383.
- Liu, W. T., 2002: Progress in scatterometer application. *J. Oceanogr.*, **58**, 121–136.
- Loehrer, S. M. T. A. Edmands, and J. A. Moore, 1996: TOGA COARE upper-air sounding data archive: development and quality control procedures. *Bull. Amer. Meteor. Soc.*, **77**, 2651–2671.
- Madden, R. A., and P. R. Julian, 1971: Detection of a 40–50 oscillation in the zonal wind in the tropical Pacific. *J. Atmos. Sci.*, **28**, 702–708.
- Maloney, E. D., and D. L. Hartmann, 2000: Modulation of eastern North Pacific hurricanes by the Madden-Julian oscillation. *J. Climate*, **13**, 1451–1460.
- Molinari, J., D. Vollaro, S. Skubis, and M. Dickinson, 2000: Origins and mechanisms of eastern Pacific tropical cyclogenesis: A case study. *Mon. Wea. Rev.*, **128**, 125–139.
- Nieto R., L. Gimeno, L. de la Torre, P. Ribera, D. Gallego, R. Garca-Herrera, J. Garca, M. Nuez, A. Redao, and J. Lorente, 2005: Climatological features of cutoff low systems in the Northern Hemisphere. *J. Climate*, **18**, 3085–3103.
- Nuss, W. A., and D. W. Titley, 1994: Use of multiquadric interpolation for meteorological objective analysis. *Mon. Wea. Rev.*, **122**, 1611–1631.
- O’Brien, J. J., 1970: Alternative solutions to the classical vertical velocity problem. *J. Appl. Meteor.* **9**, 197–203.

- Petersen, W. A., R. Cifelli, D. J. Boccippio, S. A. Rutledge, and C. Fairall, 2003: Convection and easterly wave structures observed in the eastern Pacific warm pool during EPIC-2001. *J. Atmos. Sci.*, **60**, 1754–1773.
- Raymond, D. J., C. Lopez-Carillo, and L. L. Cavazos, 1998: Case-studies of developing east Pacific easterly waves. *Quart. J. Roy. Meteorol. Soc.*, **124**, 2005–2034.
- Rogers, P. J., and R. H. Johnson, 2006: Analysis of the 13 July gulf surge event during the 2004 North American Monsoon Experiment. *Preprints, 27th Conf. on Hurricanes and Tropical Meteorology*, Amer. Meteor. Soc.
- Sadler, J. C., 1967: The tropical upper tropospheric trough as a secondary source of typhoons and a primary source of tradewind disturbances. Hawaii Institute of Geophysics Rep. 67-12, 103 pp. [Available from HIG, 2525 Correa Rd., Honolulu, HI 96822].
- Saleeby S. M., and W. R. Cotton. 2004: Simulations of the North American Monsoon System. Part I: Model analysis of the 1993 monsoon season. *J. Climate*, **17**, 1997–2018.
- Schmitz, J. T., and S. L. Mullen, 1996: Water vapor transport associated with the summertime North American monsoon as depicted by ECMWF analyses. *J. Climate*, **9**, 1621–1634.
- Stensrud, D. J., R. L. Gall, S. L. Mullen, and K. W. Howard, 1995: Model climatology of the Mexican monsoon. *J. Climate*, **8**, 1775–1793.
- Stensrud, D. J., R. L. Gall, and M. K. Nordquist, 1997: Surges over the Gulf of California. *Mon. Wea. Rev.*, **128**, 417–437.
- Straub, K. H., and G. N. Kiladis, 2002: Observations of a convectively coupled Kelvin wave in the eastern Pacific ITCZ. *J. Atmos. Sci.*, **59**, 30–53.

- Tang, M., and E. R. Reiter, 1984: Plateau monsoons of the Northern Hemisphere: A comparison between North America and Tibet. *Mon. Wea. Rev.*, **112**, 617–637.
- Thompson, R. M., Jr., S. W. Payne, E. E. Recker and R. J. Reed, 1979: Structure and properties of synoptic-scale wave disturbances in the intertropical convergence zone of the eastern Atlantic. *J. Atmos. Sci.*, **36**, 53–72.
- Thorncroft, C. D., B. J. Hoskins, and M. E. McIntyre, 1993: Two paradigms of baroclinic-wave life-cycle behavior. *Quart. J. Roy. Meteorol. Soc.*, **119**, 17–55.
- Whitfield, M. B., and S. W. Lyons, 1992: An upper-level low over Texas during summer. *Wea. Forecasting*, **7**, 89–106.
- Xu, J., X. Gao, J. Shuttleworth, S. Sorooshian, and E. Small, 2004: Model climatology of the North American Monsoon onset period during 1980-2001. *J. Climate*, **17**, 3892–3906.
- Yanai, M., S. Esbensen, and J. H. Chu, 1973: Determination of bulk properties of tropical cloud clusters from large-scale heat and moisture budgets. *J. Atmos. Sci.*, **30**, 611–627.
- Yanai, M., C. Li, and Z. Song, 1992: Seasonal heating of the Tibetan Plateau and its effects on the evolution of the Asian summer monsoon. *J. Meteor. Soc. Japan*, **70**, 319–351.

Figure Captions

Figure 1. NAME sounding network and three grids used for sounding analysis: Tier II Array (T2A), Tier I Array (T1A), and Enhanced Budget Array (EBA). Symbols indicate frequency of routine sounding launches (left number) and frequency of increased sounding launches (right number) during Intensive Observing Periods (IOPs). Budgets are computed separately for the over-water and over-land portions of the EBA.

Figure 2. Time-longitude diagram of (left) zonal wind and (right) meridional wind at 300 hPa averaged from from 25-30°N, from 1 June to 31 August 2004 and between 120-90°W. Mean westerly to easterly windshift line for 25 years is indicated. Center panel: average precipitation rate over box in Fig. 4a. Longitudes of the Enhanced Budget Array are indicated.

Figure 3. 1 July–15 August 2004 mean 300-hPa flow, 2004 height anomalies (contour interval: 5 m) from the 25-yr mean (1980-2004), and potential vorticity variance (PVU^2).

Figure 4. (a) 1 July–15 August 2004 mean precipitation rate (mm day^{-1}) using TRMM 3B42v6 product. Contour interval is 1 mm day^{-1} for rates less than 3 mm day^{-1} , then 3 mm day^{-1} above this rate. Box refers to area over which precipitation is computed for Fig. 2. Dashed lines are axes of along-Gulf (AG) and cross-Gulf (CG) cross sections shown in Figs. 12 and 14, respectively. (b) 1 July–15 August 2004 mean precipitation rate anomaly (mm day^{-1}) based on seven years of TRMM data. Contour interval is 0.5 mm day^{-1} for rates between -1 and +1 mm day^{-1} , then 1 mm day^{-1} outside this interval.

Figure 5. Time-longitude plot of 700-hPa meridional wind averaged over 15-25°N from 1 May through 30 September extending from 60 to 130°W. Tropical cyclone names are indicated.

- Figure 6. Time-longitude plot of (left) 850-hPa and (right) 200-hPa zonal wind averaged from the equator to 10°N for 1 May through 30 September extending from 60°E to 80°W. Times of prominent Gulf surges in July are indicated by S. Vertical dashed line denotes center of NAME domain. Dots refer to points of origin of tropical cyclones.
- Figure 7. 1 July–15 August 2004 mean QuikSCAT surface winds and SST.
- Figure 8. 1 July–30 September 2004 time series of (upper) Mazatlan minus Yuma surface pressure and (lower) QuikSCAT average surface wind component (southerly wind is positive) along the axis of the Gulf of California and a 2-3° coastal strip to it south. Axes of several wind and pressure difference maxima are marked along with associated tropical cyclone names at the bottom.
- Figure 9. Time series of surface pressure anomalies at three ISS sites Puerto Peñasco, Bahia Kino, and Los Mochis from 5 July to 15 August 2004. Anomalies are departures at hourly intervals from the experiment mean at each hour.
- Figure 10. Time series of precipitable water (mm) from May through September 2004 and from 15-40°N over a longitude band centered over the Gulf of California (105-115°W).
- Figure 11. 7 July–15 August 2004 zonal and meridional wind, potential temperature, and relative humidity (with respect to ice for $T < 0^{\circ}\text{C}$) (upper) mean profiles and (lower) standard deviations over land (solid) and gulf (dashed) portions of the Enhanced Budget Array. These profiles were created using the four-times daily T1A analyses.
- Figure 12. Vertical cross section along Gulf of California (position shown in Fig. 4a) of potential temperature, wind component along the plane of the section, and relative humidity averaged for the period 1 July–15 August 2004 based on two-times daily T2A analyses.
- Figure 13. 7 July–15 August 2004 mean diurnal cycle of flow from the wind profiler and surface observations at ISS site Puerto Peñasco showing nocturnal low-level jet.

- Figure 14. Vertical cross section perpendicular to the Gulf of California (position shown in Fig. 4a) of wind component in the plane of the section, divergence (10^{-5} s^{-1}), and relative humidity averaged for the period 1 July–15 August 2004 based on two-times daily T2A analyses.
- Figure 15. 7 July–15 August 2004 mean diurnal cycle of coast-perpendicular wind anomalies (departures from 24-h mean) and relative humidity at Los Mochis. This figure is based on a combination of 4 and 6-hourly soundings at this site. Tails of vectors are positioned at times of observations.
- Figure 16. Time series of zonal and meridional wind, relative humidity, and temperature deviation from the mean over the ocean portion of the Enhanced Budget Array based on four-times daily T1A analyses. Shaded periods refer to Intensive Observing Periods (IOPs).
- Figure 17. 1 July–15 August 2004 mean vertical pressure velocity at 500 hPa and TRMM 3B42v6 precipitation over the Tier II Array based on two-times daily T2A analyses.
- Figure 18. Time series of divergence, vertical pressure velocity, apparent heat source Q_1 , and apparent moisture sink Q_2 over the land portion of the Enhanced Budget Array based on four-times daily T1A analyses. Shaded periods refer to Intensive Observing Periods (IOPs).
- Figure 19. 7 July–15 August mean profiles of divergence, vertical pressure velocity, apparent heat source Q_1 , and apparent moisture sink Q_2 over the land and ocean portions of the Enhanced Budget Array based on four-times daily T1A analyses.
- Figure 20. 7 July–15 August mean profiles of divergence, vertical pressure velocity, apparent heat source Q_1 , and apparent moisture sink Q_2 over the land portion of the Enhanced Budget Array at 00, 06, 12, and 18 LT based on four-times daily T1A analyses.

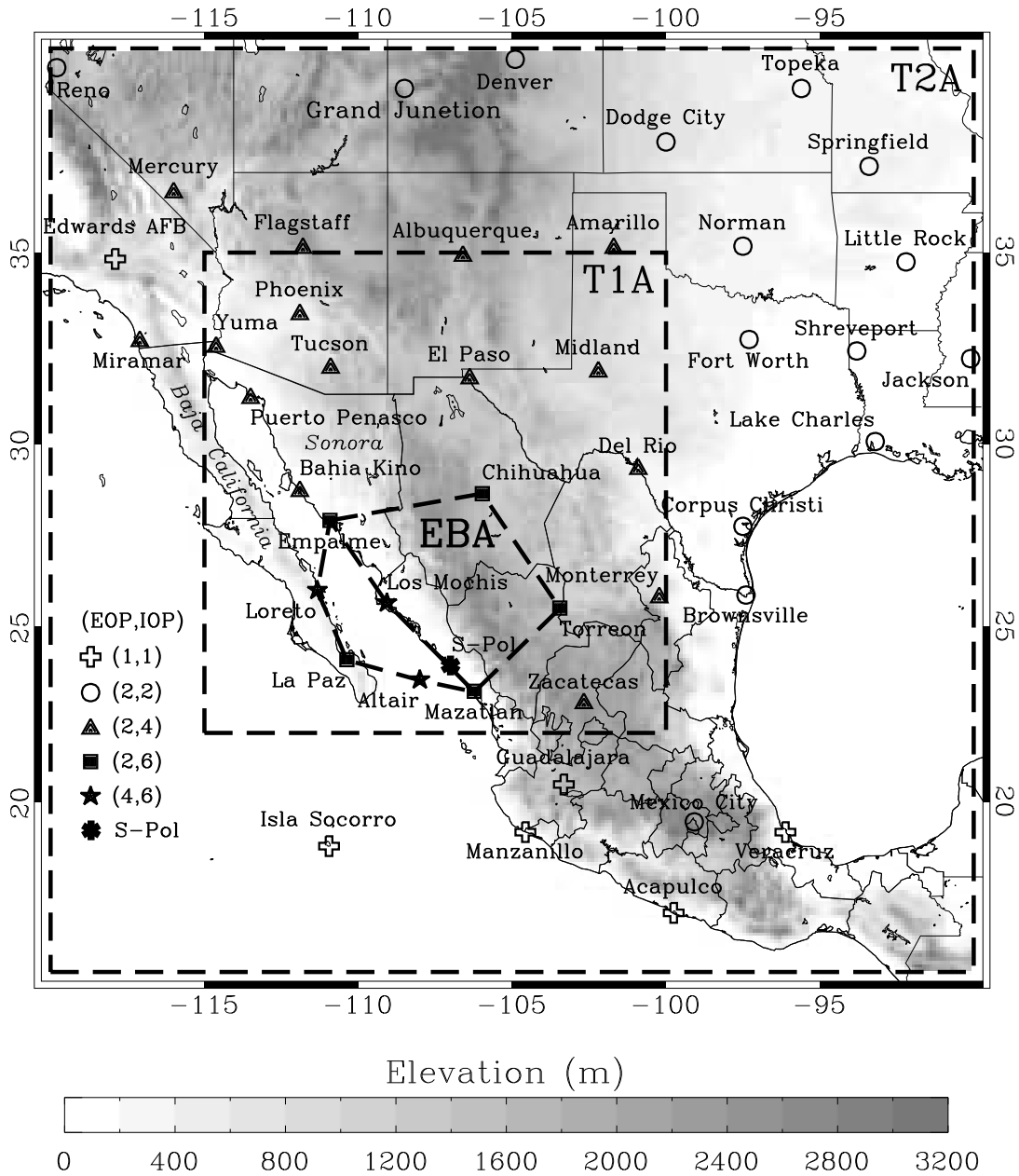


Figure 1: NAME sounding network and three grids used for sounding analysis: Tier II Array (T2A), Tier I Array (T1A), and Enhanced Budget Array (EBA). Symbols indicate frequency of routine sounding launches (left number) and frequency of increased sounding launches (right number) during Intensive Observing Periods (IOPs). Budgets are separately computed for the over-water and over-land portions of the EBA.

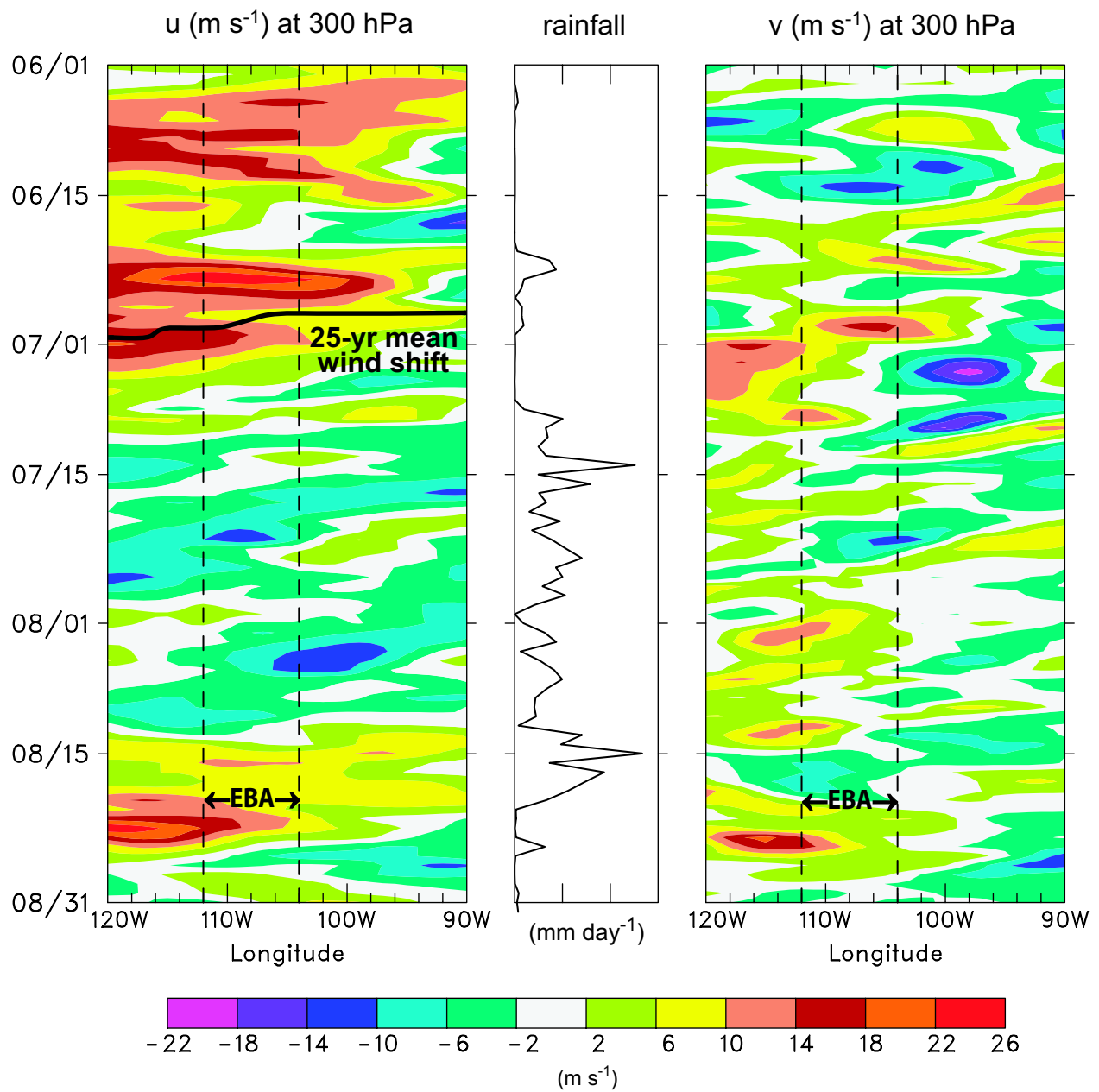


Figure 2: Time-longitude diagram of (left) zonal wind and (right) meridional wind at 300 hPa averaged from from 25-30°N, from 1 June to 31 August 2004 and between 120-90°W. Mean westerly to easterly windshift line for 25 years is indicated. Center panel: average precipitation rate over box in Fig. 4a. Longitudes of the Enhanced Budget Array are indicated.

300 hPa fields for 01 July - 15 August

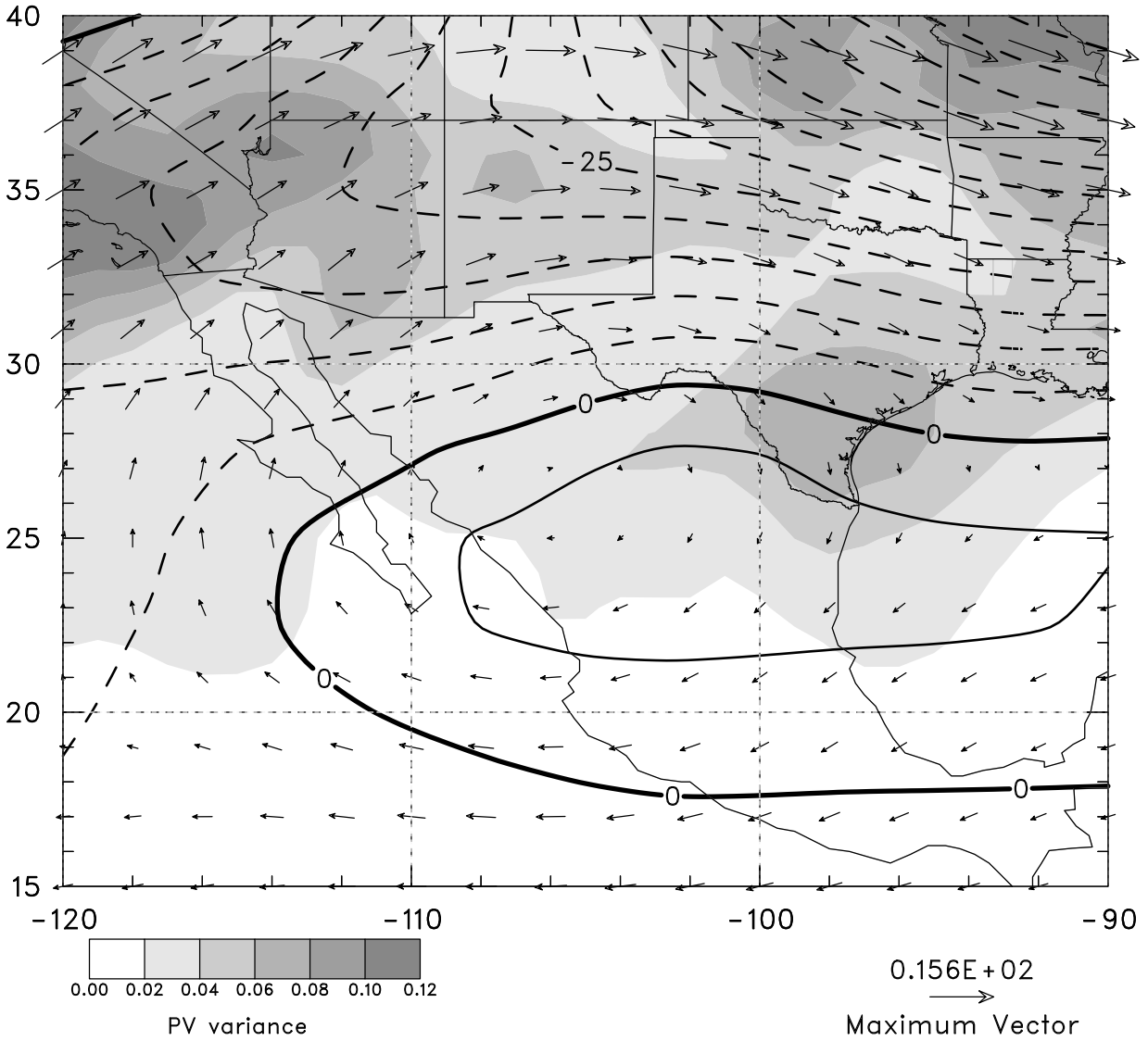


Figure 3: 1 July–15 August 2004 mean 300-hPa flow, 2004 height anomalies (contour interval: 5 m) from the 25-yr mean (1980-2004), and potential vorticity variance (PVU^2).

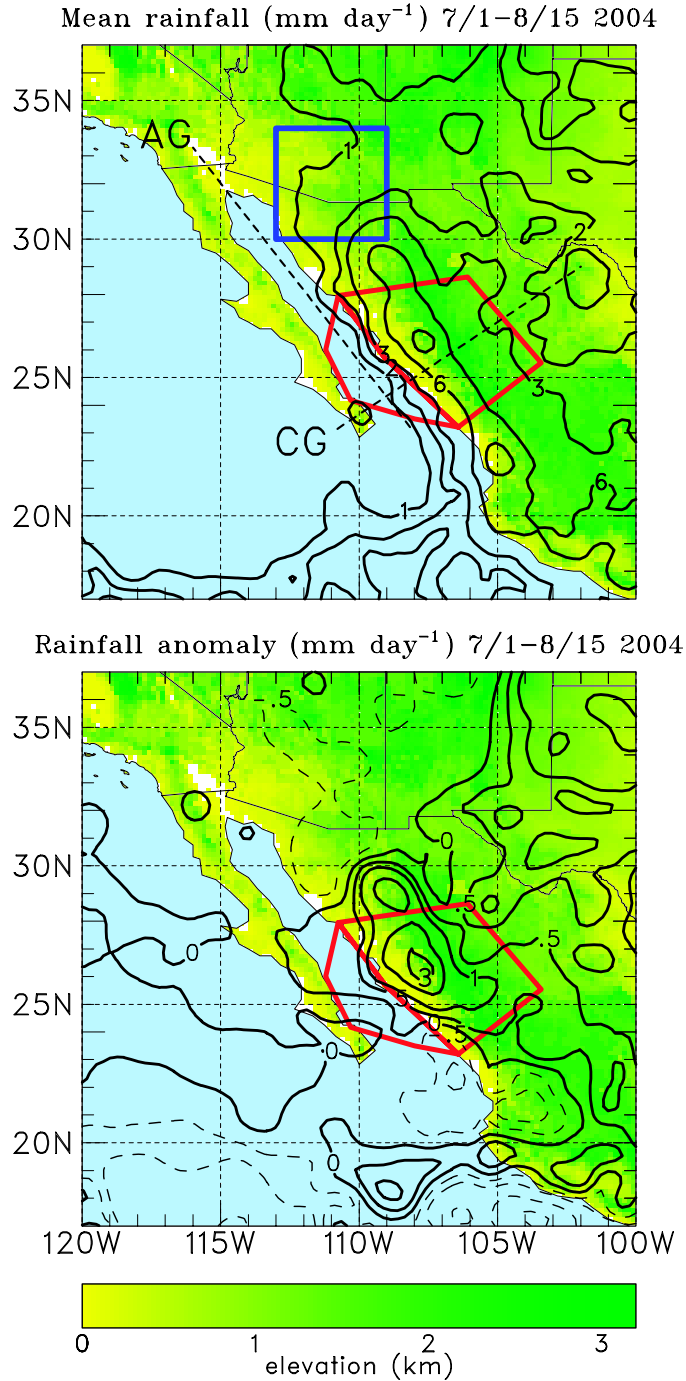


Figure 4: (a) 1 July–15 August 2004 mean precipitation rate (mm day⁻¹) using TRMM 3B42v6 product. Contour interval is 1 mm day⁻¹ for rates less than 3 mm day⁻¹, then 3 mm day⁻¹ above this rate. Box refers to area over which precipitation is computed for Fig. 2. Dashed lines are axes of along-Gulf (AG) and cross-Gulf (CG) cross sections shown in Figs. 12 and 14, respectively. (b) 1 July–15 August 2004 mean precipitation rate anomaly (mm day⁻¹) based on seven years of TRMM data. Contour interval is 0.5 mm day⁻¹ for rates between -1 and +1 mm day⁻¹, then 1 mm day⁻¹ outside this interval.

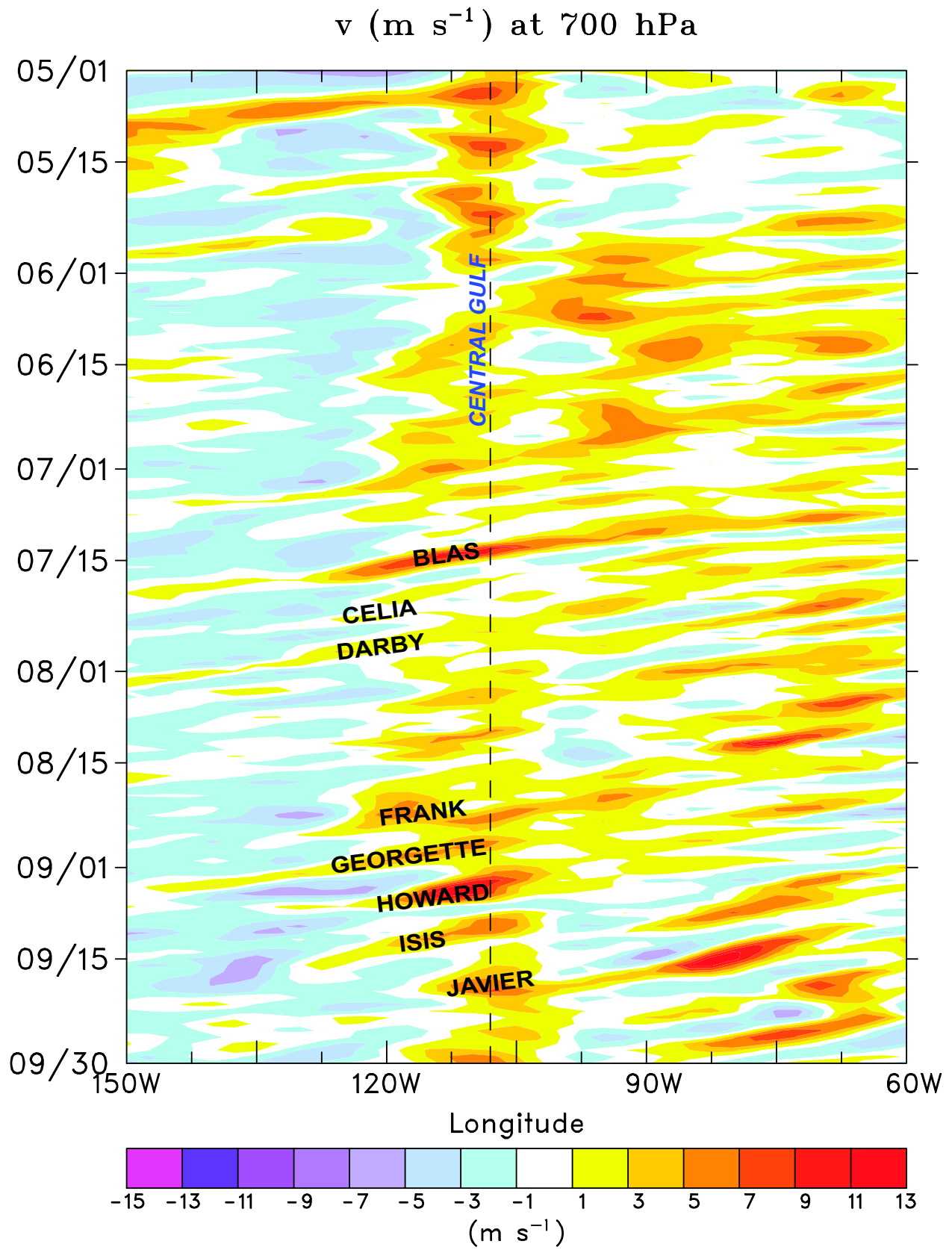


Figure 5: Time-longitude plot of 700-hPa meridional wind averaged over 15-25°N from 1 May through 30 September extending from 60 to 130°W. Tropical cyclone names are indicated.

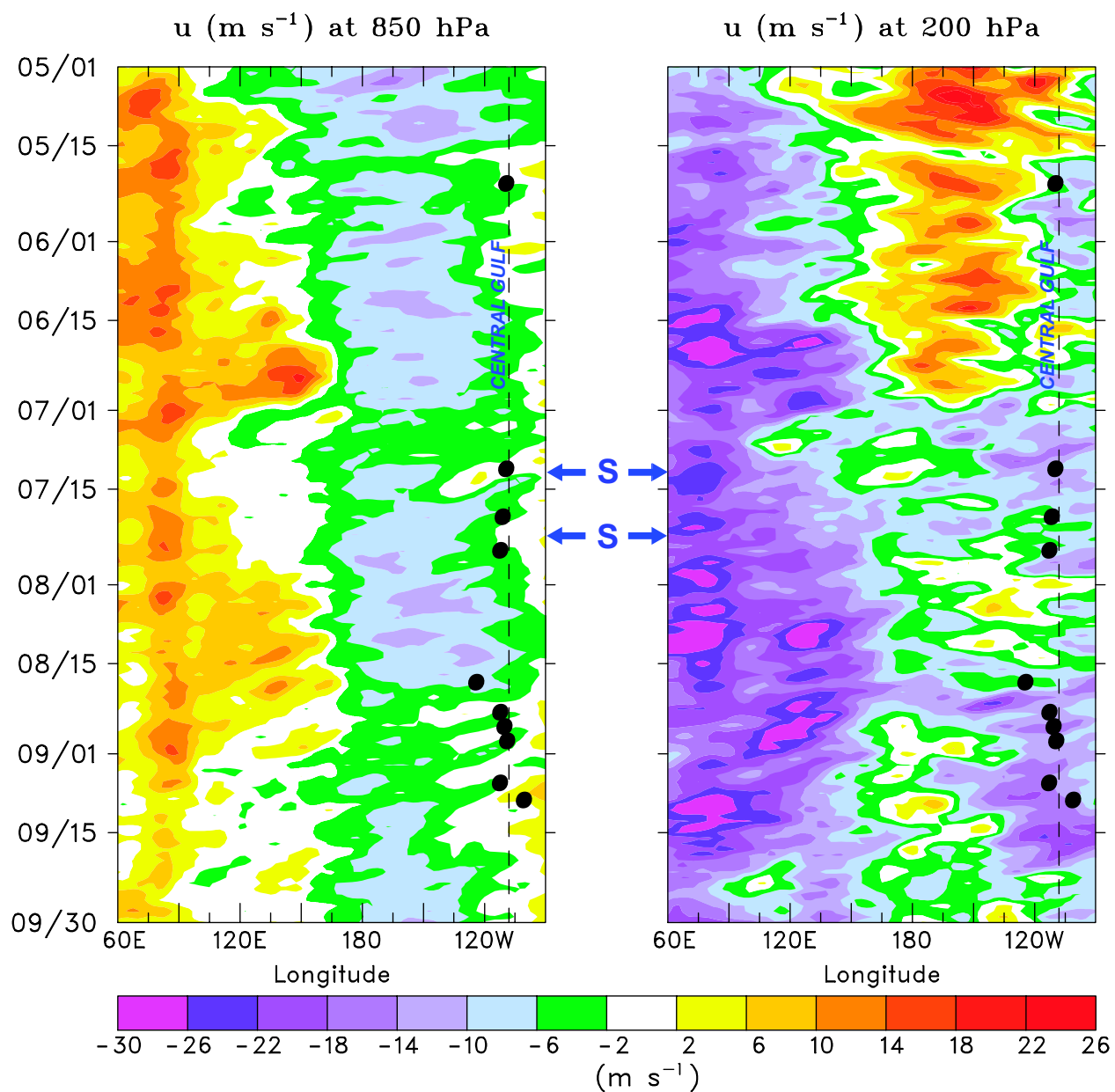


Figure 6: Time-longitude plot of (left) 850-hPa and (right) 200-hPa zonal wind averaged from the equator to 10°N for 1 May through 30 September extending from 60°E to 80°W . Times of prominent Gulf surges in July are indicated by S. Vertical dashed line denotes center of NAME domain. Dots refer to points of origin of tropical cyclones.

Sea Surface Temperature and Wind Velocity
20040701 – 20040815

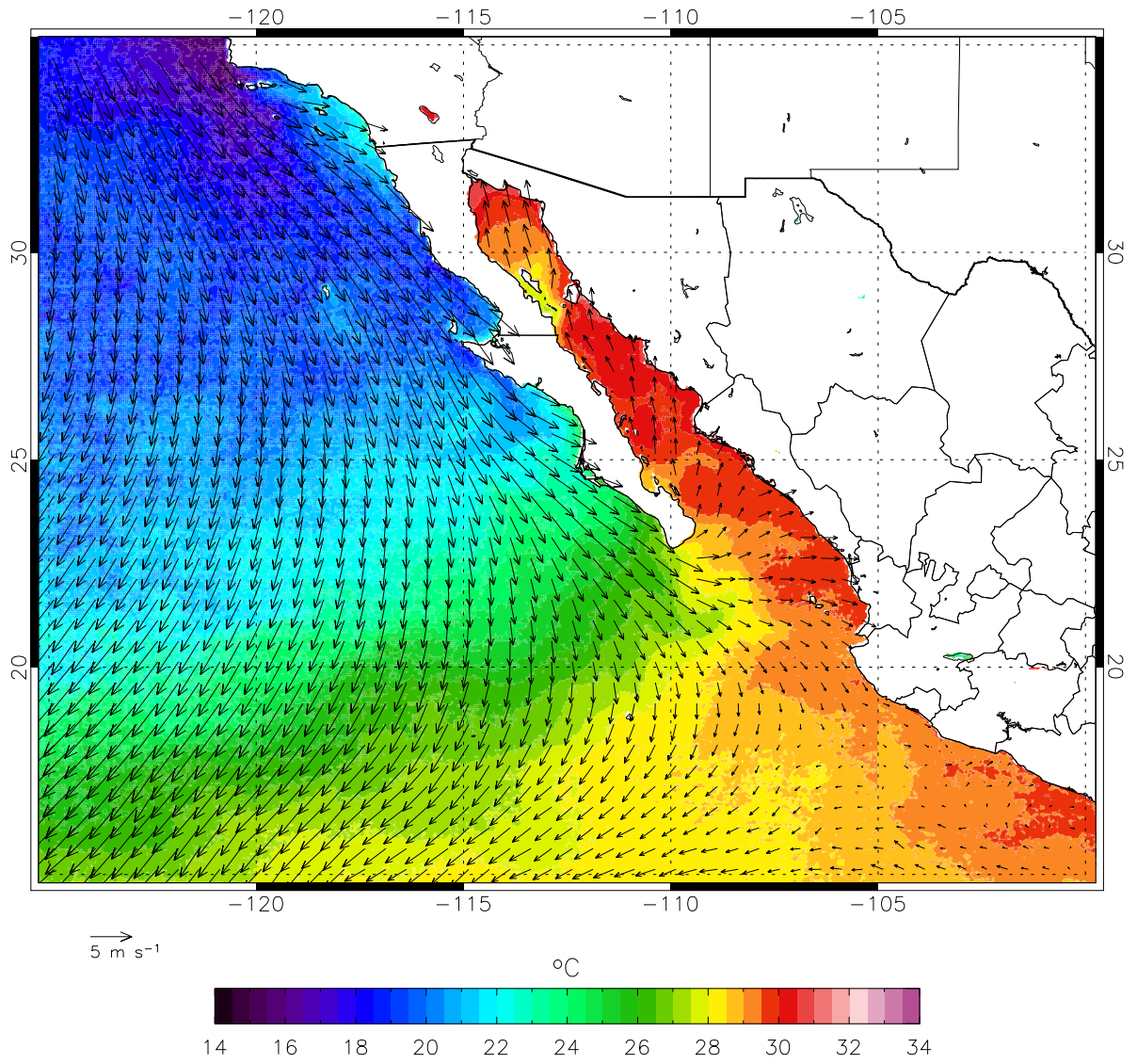


Figure 7: 1 July–15 August 2004 mean QuikSCAT surface winds and SST.

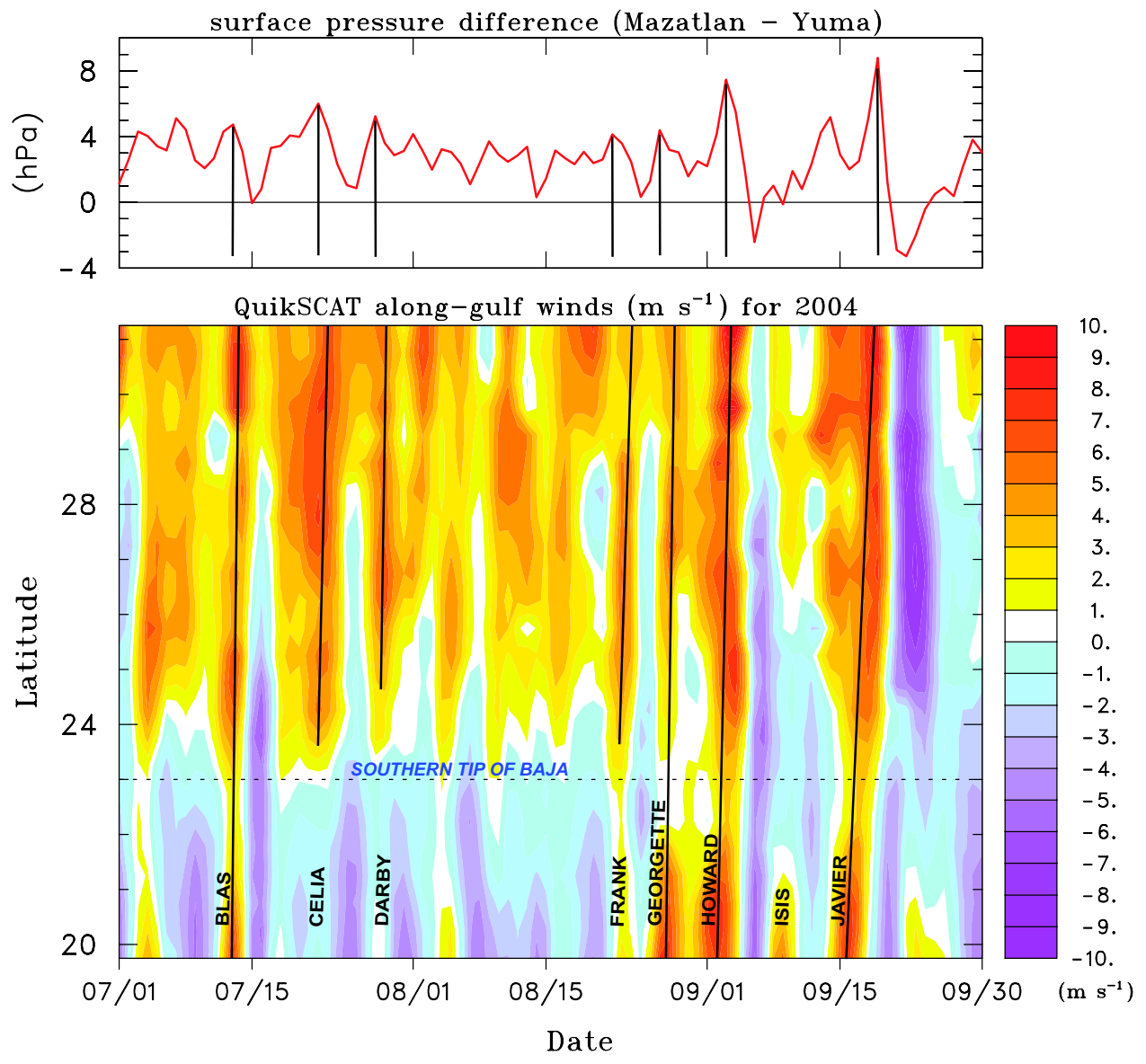


Figure 8: 1 July–30 September 2004 time series of (upper) Mazatlan minus Yuma surface pressure and (lower) QuikSCAT average surface wind component (southerly wind is positive) along the axis of the Gulf of California and a 2-3° coastal strip to it south. Axes of several wind and pressure difference maxima are marked along with associated tropical cyclone names at the bottom.

0000 UTC 5 July – 0600 UTC 15 August 2004
ISS Hourly Surface Pressure Anomalies

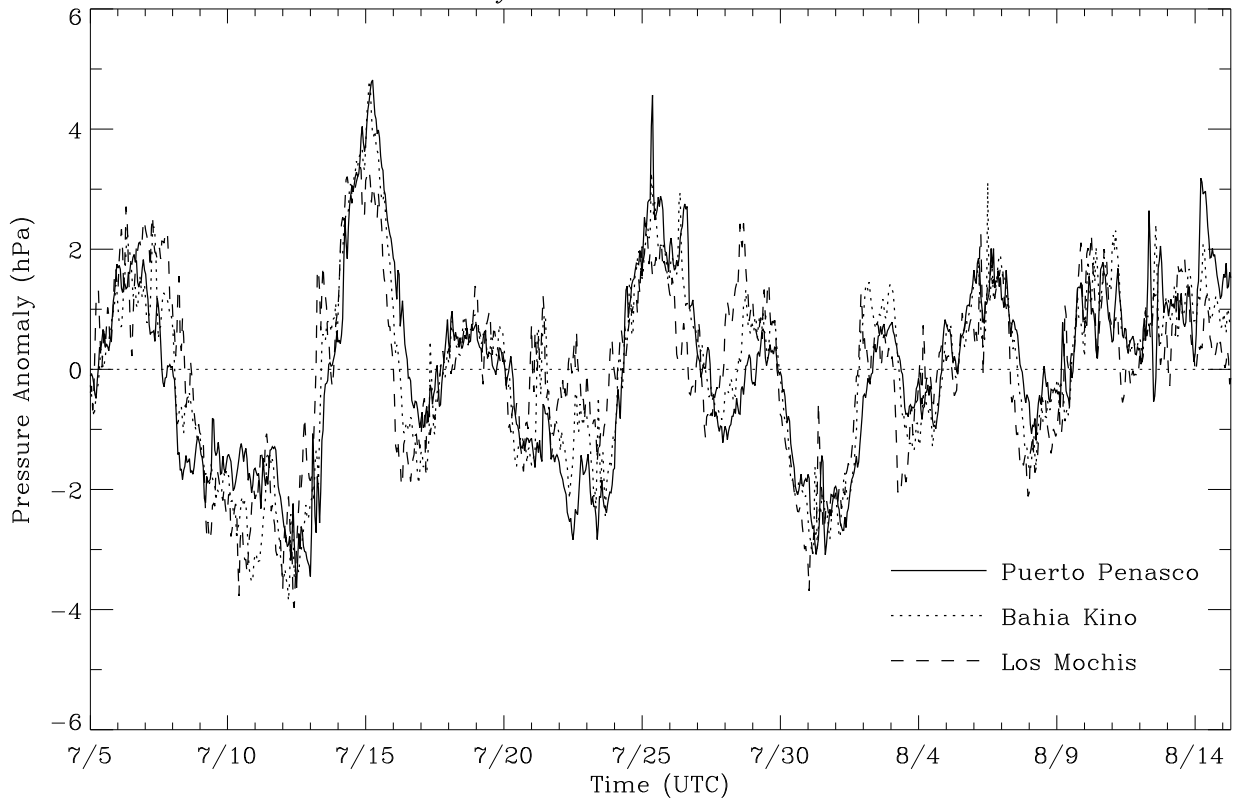


Figure 9: Time series of surface pressure anomalies at three ISS sites Puerto Peñasco, Bahia Kino, and Los Mochis from 5 July to 15 August 2004. Anomalies are departures at hourly intervals from the experiment mean at each hour.

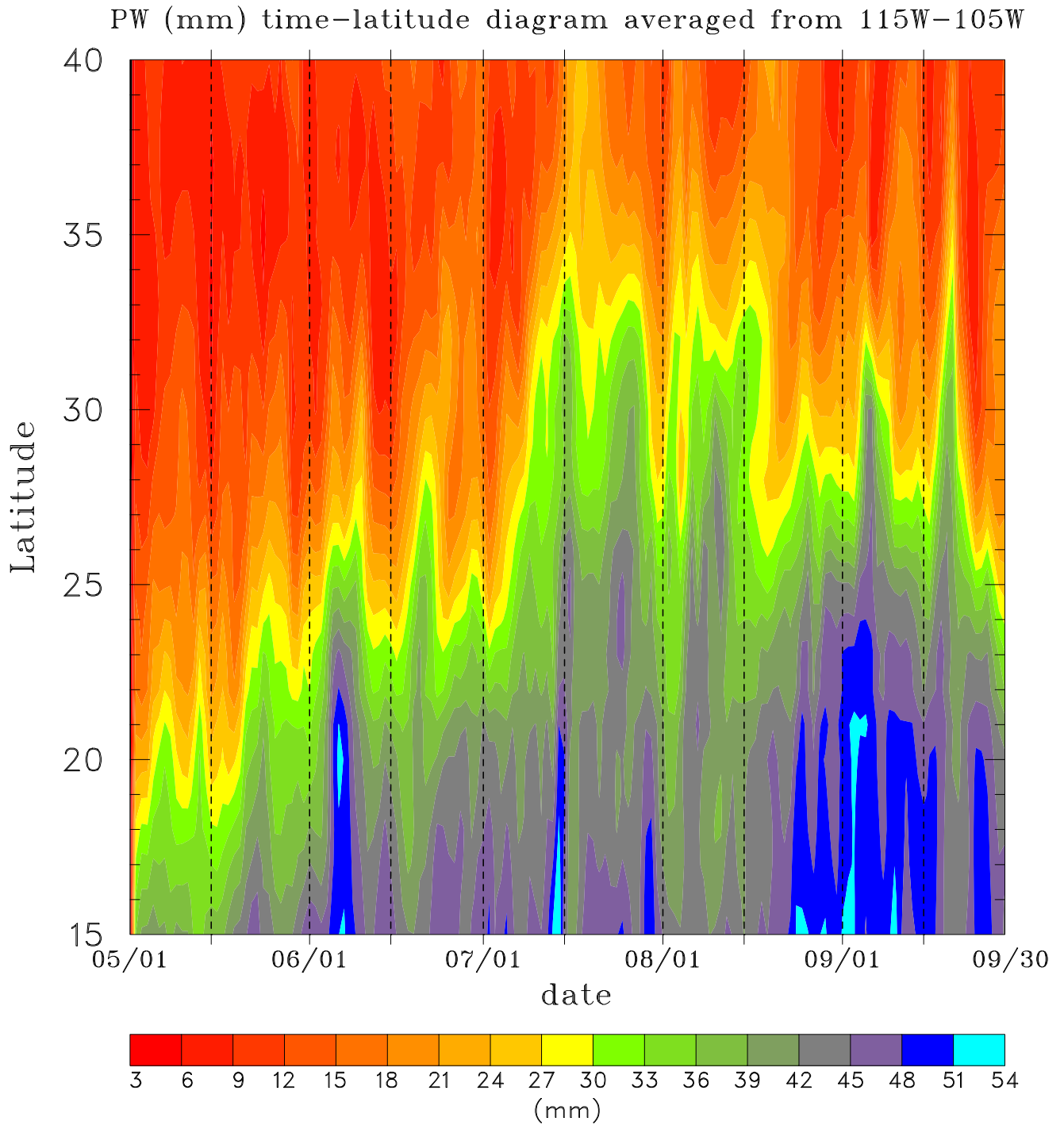


Figure 10: Time series of precipitable water (mm) from May through September 2004 and from 15-40°N over a longitude band centered over the Gulf of California (105-115°W).

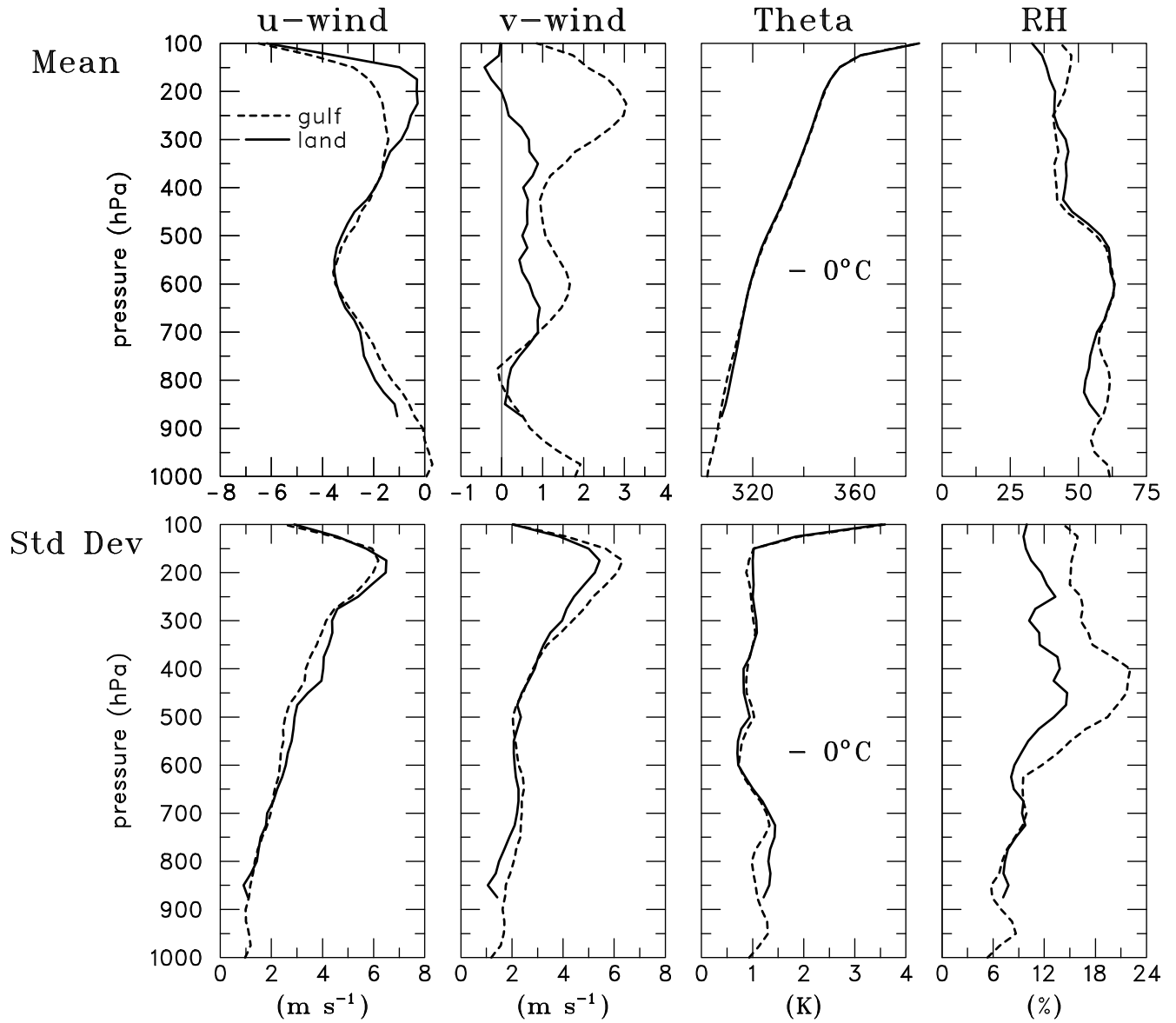


Figure 11: 7 July–15 August 2004 zonal and meridional wind, potential temperature, and relative humidity (with respect to ice for $T < 0^\circ\text{C}$) (upper) mean profiles and (lower) standard deviations over land (solid) and gulf (dashed) portions of the Enhanced Budget Array. These profiles were created using the four-times daily T1A analyses.

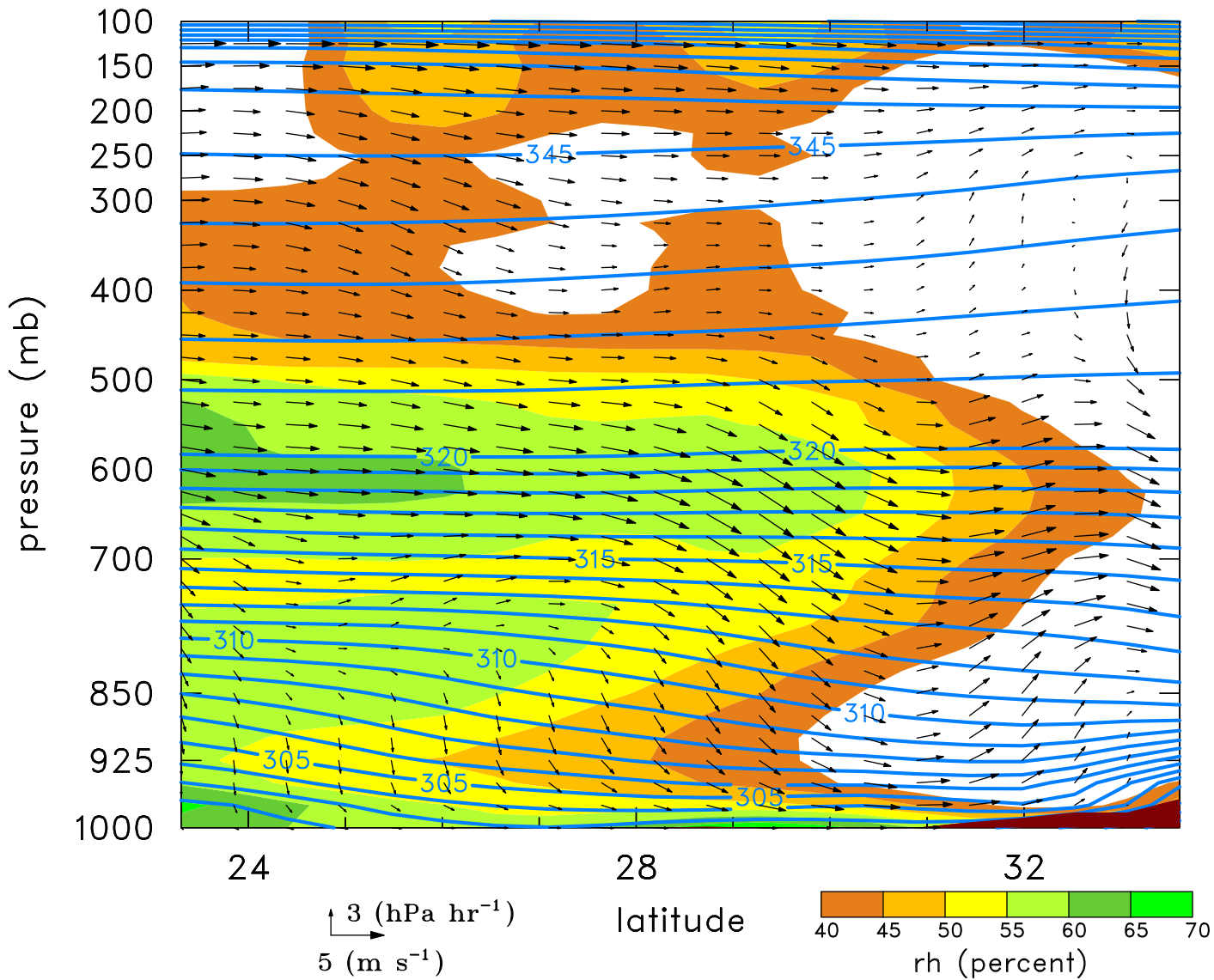


Figure 12: Vertical cross section along Gulf of California (position shown in Fig. 4a) of potential temperature, wind component along the plane of the section, and relative humidity averaged for the period 1 July–15 August 2004 based on two-times daily T2A analyses.

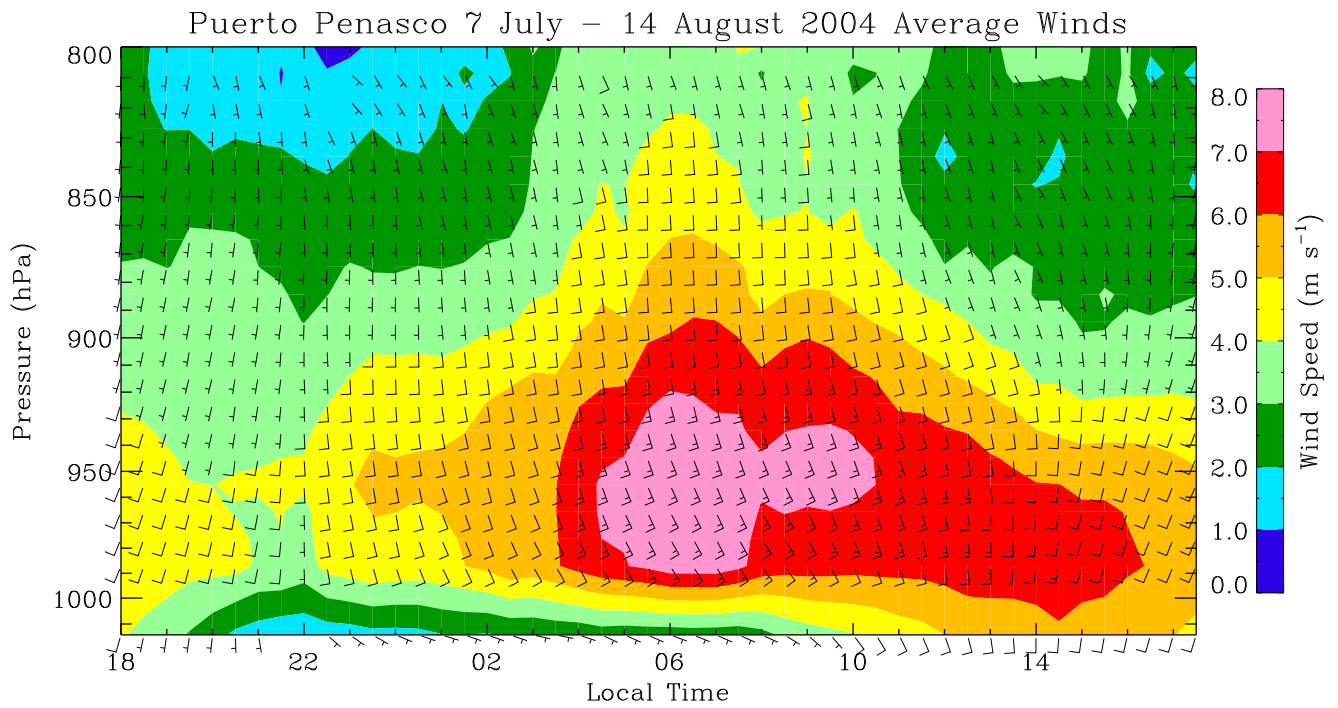


Figure 13: 7 July–15 August 2004 mean diurnal cycle of flow from the wind profiler and surface observations at ISS site Puerto Peñasco showing nocturnal low-level jet.

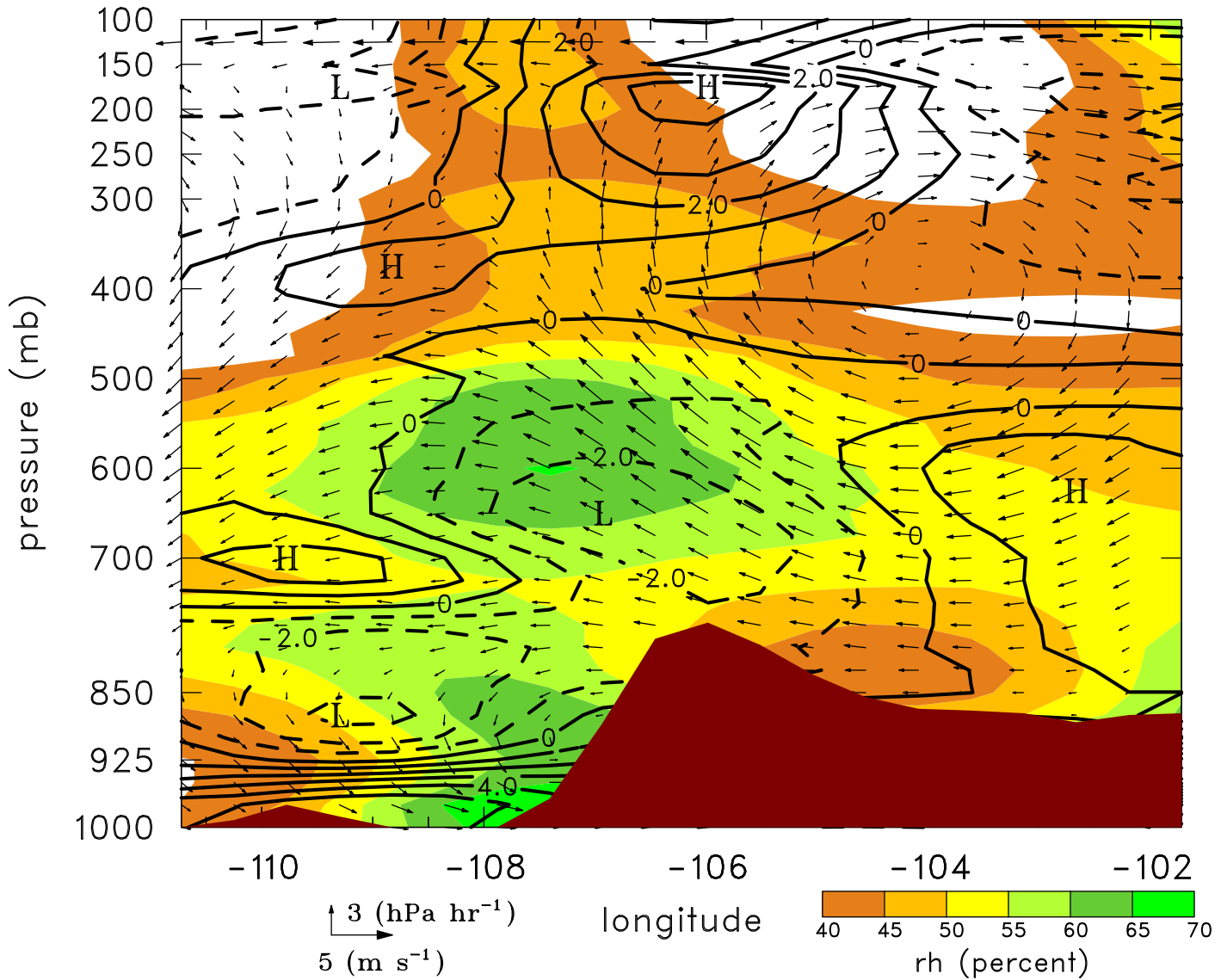


Figure 14: Vertical cross section perpendicular to the Gulf of California (position shown in Fig. 4a) of wind component in the plane of the section, divergence (10^{-5} s^{-1}), and relative humidity averaged for the period 1 July–15 August 2004 based on two-times daily T2A analyses..

Diurnal cycle of cross-gulf winds and RH at Los Mochis

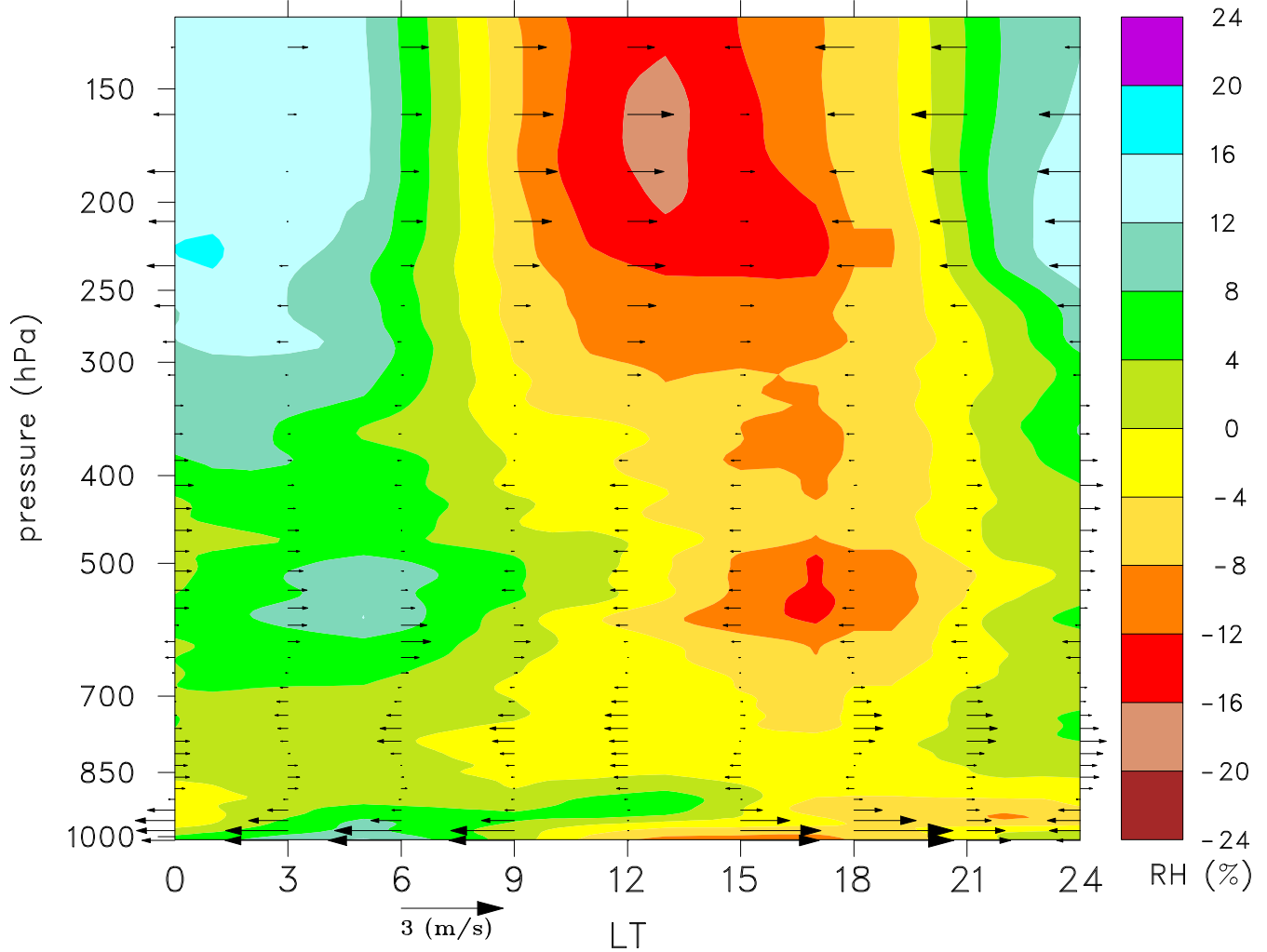


Figure 15: 7 July–15 August 2004 mean diurnal cycle of coast-perpendicular wind anomalies (departures from 24-h mean) and relative humidity at Los Mochis. This figure is based on a combination of 4 and 6-hourly soundings at this site. Tails of vectors are positioned at times of observations.

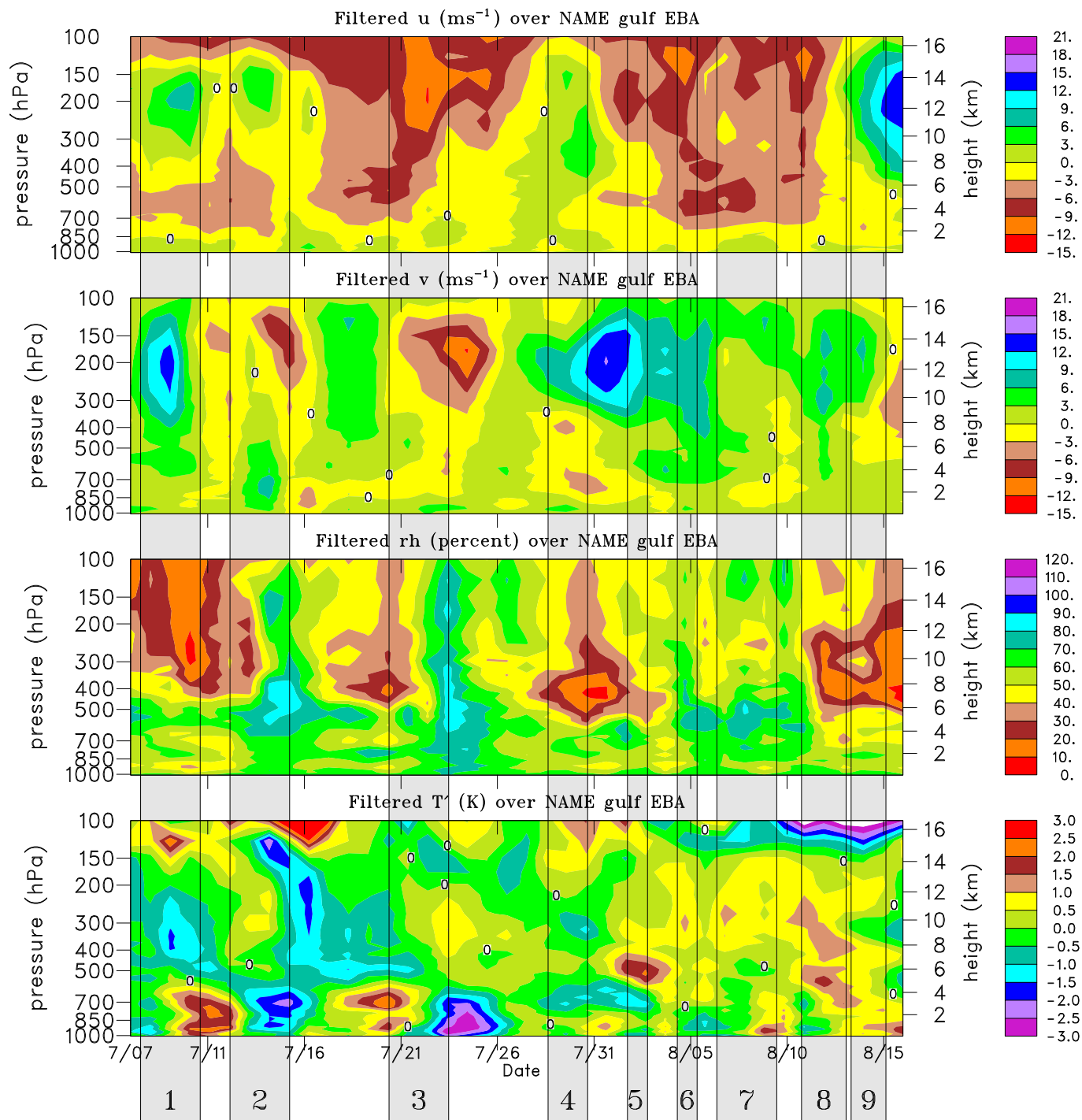


Figure 16: Time series of zonal and meridional wind, relative humidity, and temperature deviation from the mean over the ocean portion of the Enhanced Budget Array based on four-times daily T1A analyses. Shaded periods refer to Intensive Observing Periods (IOPs).

Rainfall and 500 hPa vertical motion for 1 July - 15 Aug. 2004

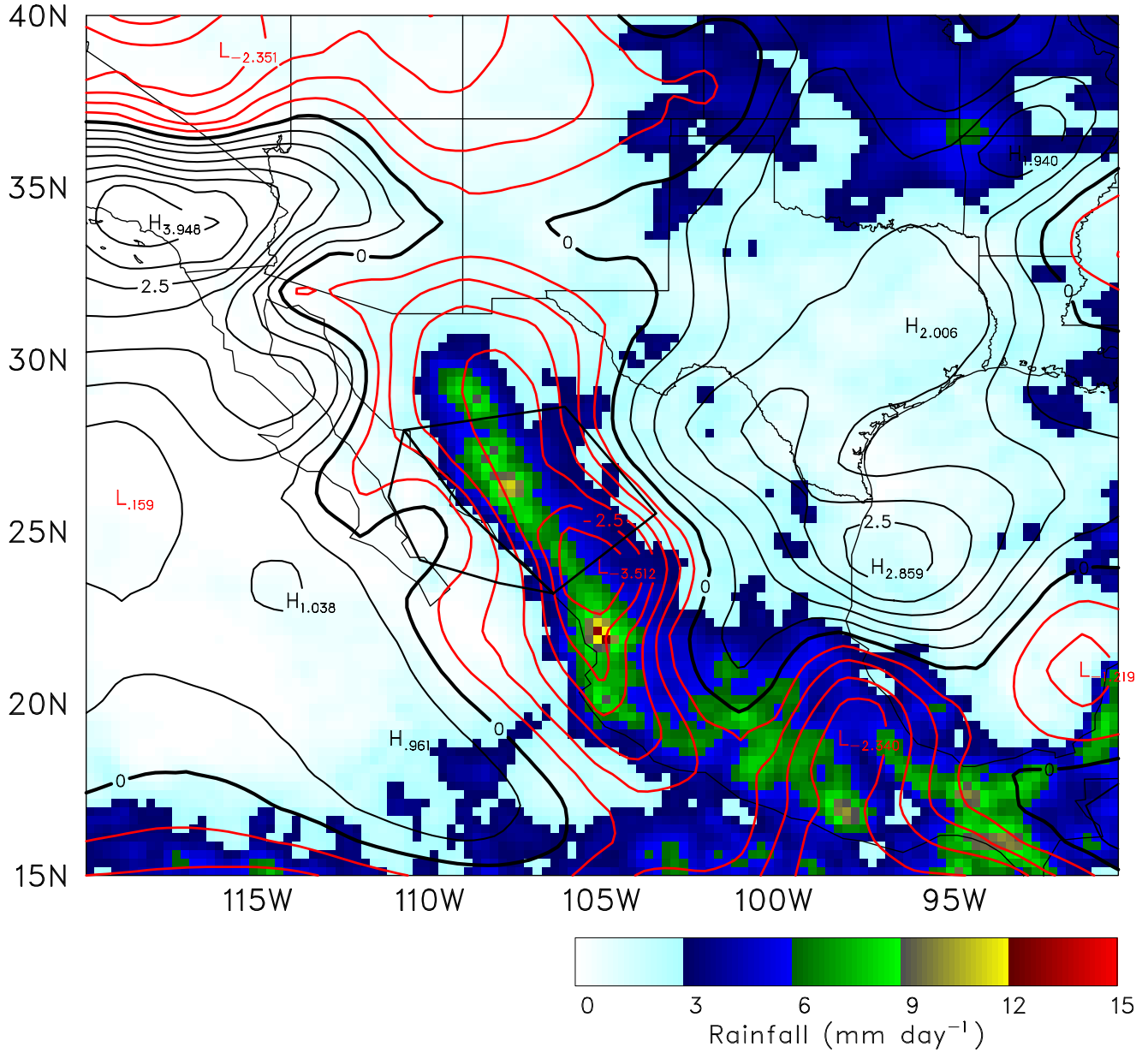


Figure 17: 1 July–15 August 2004 mean vertical pressure velocity at 500 hPa and TRMM 3B42v6 precipitation over the Tier II Array based on two-times daily T2A analyses.

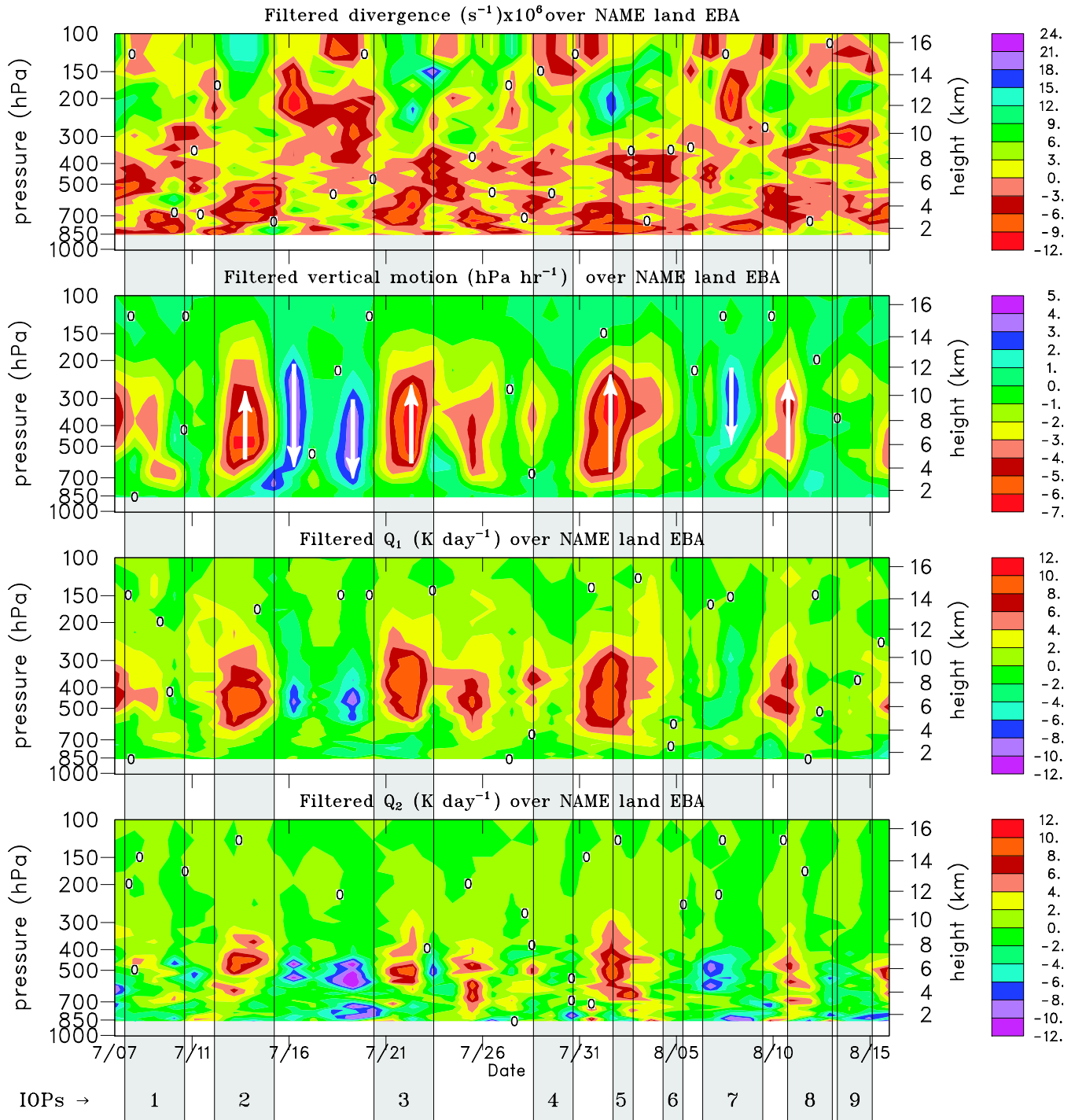


Figure 18: Time series of divergence, vertical pressure velocity, apparent heat source Q_1 , and apparent moisture sink Q_2 over the land portion of the Enhanced Budget Array based on four-times daily T1A analyses. Shaded periods refer to Intensive Observing Periods (IOPs).

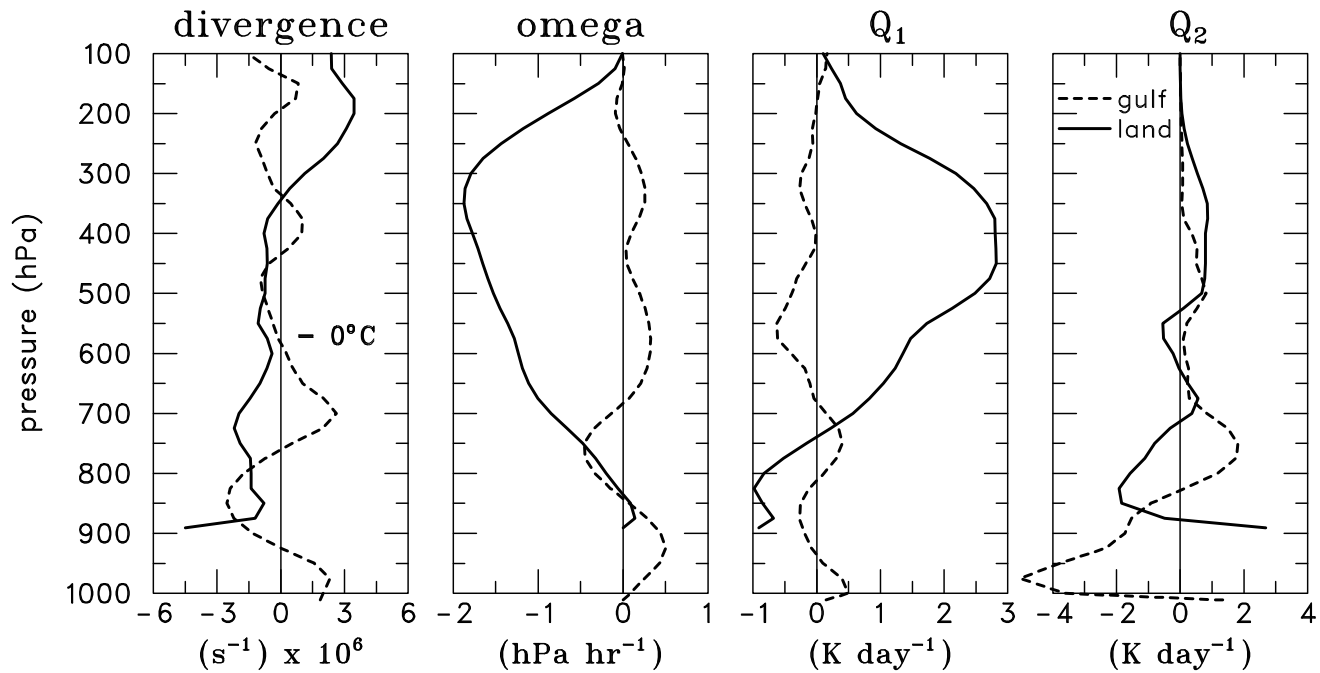


Figure 19: 7 July–15 August mean profiles of divergence, vertical pressure velocity, apparent heat source Q_1 , and apparent moisture sink Q_2 over the land and ocean portions of the Enhanced Budget Array based on four-times daily T1A analyses.

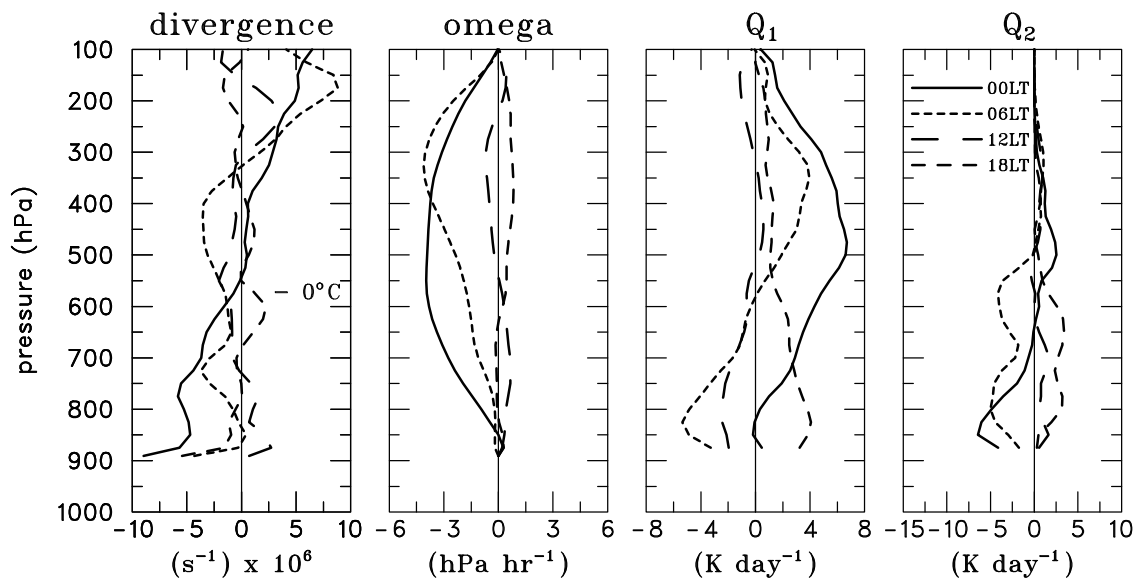


Figure 20: 7 July–15 August mean profiles of divergence, vertical pressure velocity, apparent heat source Q_1 , and apparent moisture sink Q_2 over the land portion of the Enhanced Budget Array at 00, 06, 12, and 18 LT based on four-times daily T1A analyses.